

**REPUBLIC OF TURKEY
YILDIZ TECHNICAL UNIVERSITY
GRADUATE SCHOOL OF NATURAL AND APPLIED SCIENCES**

**STRUCTURAL ANALYSIS OF ABELL 2554
GALAXY CLUSTER**

MUHAMMED KIYAMI ERDİM

**MSc. THESIS
DEPARTMENT OF PHYSICS
PROGRAM OF PHYSICS**

**ADVISER
ASSIST. PROF. DR. MURAT HÜDAVERDİ**

İSTANBUL, 2016

REPUBLIC OF TURKEY
YILDIZ TECHNICAL UNIVERSITY
GRADUATE SCHOOL OF NATURAL AND APPLIED SCIENCES

**LOCATION ANALYSIS OF THE EMERGENCY SERVICE
CENTERS OF A CASE COMPANY**

A thesis submitted by Muhammed Kıyami ERDİM in partial fulfillment of the requirements for the degree of **MASTER OF SCIENCE** is approved by the committee on 27.04.2016 in Department of Physics.

Thesis Adviser

Assist. Prof. Dr. Murat HÜDAVERDİ
Yıldız Technical University

Approved By the Examining Committee

Assist. Prof. Dr. Murat HÜDAVERDİ
Yıldız Technical University

Assoc. Prof. Dr. Taylan YETKİN
Yıldız Technical University

Prof. Dr. E. Nihal ERCAN
Bogazici University



This study was supported by the BAPK Grant No: 2015-01-01-KAP05

This study was supported by the Scientific and Technological Research Council of Turkey (TUBITAK) Grant No: 113F117

ACKNOWLEDGEMENTS

First, I would like to thank my research supervisor for his advice and consultation, Assistant Prof. Murat HÜDAVERDİ. Without his assistance throughout the process, this paper would have never been accomplished. I would like to thank you very much for your support and understanding over these time.

I would also like to show gratitude our laboratory partners, including Turgay ÇAĞLAR, Hakan SERT, Onur ÜNVER and Nergis CESUR.

April, 2016

Muhammed Kıyami ERDİM

TABLE OF CONTENTS

	Page
LIST OF SYMBOLS	vii
LIST OF ABBREVIATIONS.....	viii
LIST OF FIGURES	ix
LIST OF TABLES.....	xii
ABSTRACT	xiii
ÖZET	xiii
CHAPTER 1	
INTRODUCTION	1
1.1 Literature Review	1
1.1.1 Clusters of Galaxies	1
1.1.2 Cluster Mergers	1
1.2 Objective of Thesis	4
1.3 Hypothesis	4
CHAPTER 2	
CHANDRA OBSERVATORY	5
2.1 General Information.....	5
2.2 Technical Description.....	6
2.3 Instruments	6
CHAPTER 3	
OBSERVATION AND DATA REDUCTION.....	13
3.1 Abell 2554	13
3.2 Data Reduction	15
CHAPTER 4	
ANALYSIS.....	17

4.1 Overview.....	17
4.1.1 X-ray Images of A2554	17
4.1.2 Surface Brightness Profile	18
4.2 Spectral Analysis	22
4.3 Hardness-Ratio Map	24
4.4 Temperature Map.....	25
4.5 Pressure and Entropy Map.....	28
4.6 Radio and Optic Observations	29

CHAPTER 5

RESULTS AND DISCUSSION.....	30
5.1 Merger Signatures.....	30
5.2 Merger Shock.....	33
5.3 Cold Front.....	36
5.4 Conclusion	37
REFERENCES	39
CURRICULUM VITAE.....	41

LIST OF SYMBOLS

γ	Adiabatic Index
ρ	Density
H_0	Hubble Constant
nH	Hydrogen Column Density
M_ρ	Mach Number
z	Redshift

LIST OF ABBREVIATIONS

arcmin	Arc-minute
arcsec	Arc-second
Dec.	Declination
dof	Degrees of freedom
ICM	Intra Cluster Medium
kpc	Kiloparsec
Mpc	Megaparsec
nH	Hydrogen Column Density
NVSS	NRAO VLA Sky Survey
R.A.	Right Ascension
SAO-DSS	SAO Digitized Sky Survey
VLA	Very Large Array

LIST OF FIGURES

		Page
Figure 2.1	Chandra X-ray Observatory (CXO)	5
Figure 2.2	CXO Instruments.....	6
Figure 2.3	Advanced CCD Imaging Spectrometer (ACIS)	7
Figure 2.4	High Resolution Camera (HRC) Illustration.....	8
Figure 2.5	HRC.....	8
Figure 2.6	ACIS.....	9
Figure 2.7	Transmission Gratings.....	10
Figure 2.8	Chandra Grating Spectrometers	11
Figure 3.1	X-ray image of the trio-clusters A2550, A2554 and A2556	13
Figure 3.2	X-ray image of A2554.....	15
Figure 4.1	All band x-ray image of A2554 (filtered)	17
Figure 4.2	Soft x-ray image (left), hard x-ray image (right) of A2554	18
Figure 4.3	Selected regions for surface brightness profile	19
Figure 4.4	Surface brightness profile (whole cluster).....	19
Figure 4.5	Surface brightness profile (region 1).....	20
Figure 4.6	Surface brightness profile (region 2).....	20
Figure 4.7	Surface brightness profile (region 3).....	21
Figure 4.8	Surface brightness profile (whole cluster & region 1)	21
Figure 4.9	The regions used for spectrum extraction (black) and the selected background region (white).....	22
Figure 4.10	Spectrum of A2554	23
Figure 4.11	Radial temperature distribution.....	23
Figure 4.12	X-ray image (left) and hardness-ratio map (right) of A2554	25

Figure 4.13	Selected regions for confirmation of the hardness-ratio/temperature relation	25
Figure 4.14	Temperature values of the regions in Figure 4.13.....	26
Figure 4.15	Hardness-ratio and temperature relation of A2554.....	27
Figure 4.16	Temperature map of A2554	27
Figure 4.17	Pressure map (left) and entropy map (right) of A2554	28
Figure 4.18	X-ray image with radio contours (left) and radio image (right) of A2554.....	29
Figure 4.19	Optic image of A2554	29
Figure 5.1	Surface brightness profile with discontinuities	31
Figure 5.2	Temperature map with discontinuity regions (White colored)	31
Figure 5.3	Surface brightness profile of region 1 (showed in Figure 4.3) with discontinuities	32
Figure 5.4	Temperature map with discontinuity regions for region1(White colored)	32
Figure 5.5	Sub-structures created by possible merger activity.....	33
Figure 5.6	Temperature map with possible shock region (region 2), pre-shock region (region 3) and after shock region (region 1).....	34
Figure 5.7	Pressure and entropy map with sub-structure regions.....	35
Figure 5.8	Temperature values of Region 1, 2 and 3 showed in Figure 5.6.....	35
Figure 5.9	Pseudo-pressure map with possible cold-front.....	36
Figure 5.10	Pseudo-entropy map with possible cold-front.....	37

LIST OF TABLES

	Page
Table 3.1 Information about galaxy cluster A2554	14
Table 4.1 Spectral values for analyzed regions	24



ABSTRACT

STRUCTURAL ANALYSIS OF ABELL 2554 GALAXY CLUSTER

Muhammed Kiyami ERDİM

Department of Physics

MSc. Thesis

Adviser: Asist. Prof. Dr. Murat HÜDAVERDİ

As far as we know, clusters of galaxies are the biggest organized structures in the universe. Because of this, understanding the evolution and inner dynamics of clusters may lead us to understand basic principles of the universe. Observing the merging clusters is a very good way to do that. Because clusters evolve with mergers. Merging event also disrupts the relaxed state of clusters, so we can identify the behaviors of them. Non-symmetric morphology and temperature distributions are essential clues for diagnosing the mergers. We can also find answers about the process itself. Most of the radiation that comes from the plasma in clusters are in x-ray band, which makes x-ray observations essential. Because of this we used observations of CHANDRA X-RAY OBSERVATORY. The main object of this thesis is to find out the properties of galaxy cluster Abell 2554, which is thought to be in a merging process.

Key words: Galaxy, Hot Plasma, Clusters of Galaxies, Mergers, X-rays, Satellite

YILDIZ TECHNICAL UNIVERSITY
GRADUATE SCHOOL OF NATURAL AND APPLIED SCIENCES

ABELL 2554 GALAKSİ KÜMESİNİN YAPISAL ÖZELLİKLERİ

Muhammed Kıyami ERDİM

Fizik Bölümü

Yüksek Lisans Tezi

Tez Danışmanı: Asist. Prof. DR. Murat HÜDAVERDİ

Bildiğimiz kadarı ile, galaksi kümeleri evrendeki en büyük organize yapılardır. Bu sebeple kümelerin evrimini ve iç dinamiklerini anlamak, evrenin temel prensiplerini anlamamıza yol açabilir. Birleşen kümeleri gözlemlemek bu iş için çok uygundur. Çünkü kümelerin evrimi birleşmeler ile gerçekleşir. Birleşme olayı kümelerin durgun yapılarını bozduğu için bu durum karşısındaki davranış biçimlerini tanımlayabiliriz. Simetrik olmayan şekilleri ve sıcaklık dağılımları tanı koymak açısından çok önemli ipuçlarıdır. Bunlar ile ayrıca sürecin kendisi hakkında da cevaplar bulabiliriz. Küme plazmasının yaptığı ışımanın çoğu x-ışını bandındadır. X-ışını gözlemleri bu açıdan büyük önem taşır. Bu sebeple çalışmamızda CHANDRA isimli x-ışını uydusunun gözlemlerini kullandık. Bu tezin esas amacı, bir birleşme süreci içerisinde bulunduğunu düşündüğümüz Abell 2554 galaksi kümesinin özelliklerini belirlemektir.

Anahtar Kelimeler: Galaksi, Sıcak Plazma, Galaksi Kümeleri, Birleşme, X-ray, Uydu

INTRODUCTION

1.1 Literature Review

In this chapter, we presented the literature review of clusters of galaxies and mergers.

1.1.1 Clusters of Galaxies

Clusters of galaxies are the most massive gravitationally bounded structures in the universe. According to the standard cold dark matter model, they evolve with mergers through filaments [1]. They may contain thousands of galaxies. But the galaxies correspond to a very low percentage of their total baryonic mass. Most of their baryonic mass originates from hot plasma that fills the gap between galaxies, called intra-cluster medium (ICM).

1.1.2 Clusters Mergers

Cluster mergers are the mechanism by which clusters are assembled. In these mergers, the sub-clusters collide at velocities $\sim 2000\text{km/s}$, releasing gravitational binding energies of as much as $\geq 10^{64}$ ergs. During mergers, shocks are driven into the intra-cluster medium [2]. Merger shocks should heat and compress the x-ray emitting intra-cluster gas, and increase its entropy. We also expect that particle acceleration by these shocks will produce relativistic electrons and ions, and these can produce synchrotron radio, inverse compton extreme ultraviolet and hard x-ray, and gamma-ray emission [2].

The ICM is generally close to hydrostatic equilibrium in clusters which are not undergoing strong mergers [3]. The clusters that member of an ongoing merger often

shows strong distortion of symmetry. We can detect merger signatures by examining the ICM. Both observations and simulations show that cluster mergers change the physical characteristics of ICM physics, such as thermal conduction, viscosity, self-interaction of dark matter and particle acceleration [4]. Observations of cluster mergers have proven valuable also in constraining the nature of dark matter [5].

Radiation of the ICM corresponds to x-ray band, so, observations of x-ray observatories are used for analysis. Early X-ray observations of cluster mergers using ROSAT and ASCA satellites revealed a hot, apparently shock-heated ICM in regions affected by merger activity [6]. However, the spatial resolution was not sufficient to see the surface brightness edge expected due to the compression of gas at the shock front. The launch of the Chandra X-Ray Observatory with its sub-arcsec resolution and excellent sensitivity was expected to reveal many shock edges in merging clusters [5].

With this improvement in angular resolution, previously unseen, or rarely seen, phenomena have been detected in many clusters. The surprising “edges”, the boundaries between cold clouds traversing cluster cores, which Chandra has shown are a common feature of clusters [7]. Firstly, they were thought to be merger shocks. But when the temperature measurements were made, it was understood that these edges were something else. This new phenomena is called “Cold Front”. These “cold fronts” mark the boundary of cool, dense core of gas that is moving through the warmer ambient medium [8]. Cold fronts are thought to be the remnants of the cool cores of the two merging subclusters. They survived shocks and mixing of a merger [9].

Dynamical activities triggered by mergers often produce contact discontinuities between gases of different entropies that can be seen as surface brightness edges in X-ray observations [4]. An additional signature is the heating of the cluster gas in the interaction region. Also substructures can be detected. Recent x-ray observations have shown substructure in the ICM in the form of shocks, cold fronts and gas sloshing spirals. These all appear as surface brightness discontinuities in the x-ray images [1]. They can be differentiated with some aspects, like gradients of pressure, density and temperature profiles across the region.

About differentiation of the cold fronts, one hint is given by the gas pressure profiles across the edges, which show that there is approximate pressure equilibrium across the density discontinuity as opposed to a large pressure jump expected in a shock front [9]. Secondly, denser side of the density jump is colder in cold fronts while it is the opposite in shocks.

Shocks in clusters are consequences of large-scale cluster mergers, or sometimes of outbursts from the central AGNs. The temperature, density and pressure all change across a shock front. Typical cluster merger shocks have Mach numbers $M \leq 3$ [1]. Mach number is a value that shows the sharpness of the changed property while crossing the shock region. The Bullet Cluster provides a textbook example of such a merger shock in the ICM. In cold fronts and sloshing spirals, only the density and temperature change across the surface brightness discontinuity, while the pressure does not, in contrast to shocks. Also, in both merger and sloshing cold fronts the gas on the denser side of the front is cooler, whereas in shocks the denser gas is hotter [1].

In merger process, while the dense and cold cloud move through the less dense and warmer ambient gas, it is slowed by ram pressure. In the decelerating reference frame of the cloud, there is an inertial force directed from the dense phase to the less dense phase, which makes the front interface of the cloud Rayleigh-Taylor (RT) unstable [9]. If the cloud is stable, there should be enough gravitational force to prevent the RT instability. Calculations showed that the gravity of the gas itself is insufficient to suppress the RT instability. Because the front is apparently stable, this means that there has to be a massive underlying dark matter subcluster, centered inside the front, that holds the gas cloud together. This is, of course, what we expect in a merger. If the total mass of the underlying dark matter halo is the usual factor of ~ 10 higher than the gas mass, its gravity at the front surface would be more than sufficient to compensate for drag force, thereby removing the RT instability condition. Furthermore, because the density is not constant inside the cool gas along the front, there has to be an underlying mass concentration that supports the resulting pressure gradient [9]. These results show the strong correlation between dark matter and cold fronts. Mass and dark matter distributions calculated with lensing also

support the idea that the cold fronts co-moving with a dark matter clump. The observed temperature jumps at cold fronts require that thermal conduction across the fronts is strongly suppressed [9].

A2554 shows strong distortion with its x-ray image and temperature distribution. There are several surface brightness discontinuities that corresponds to temperature jumps. In this work we tried to show the merger signatures, identify the specific distorted regions and diagnose them. Cosmological parameters that we assume are $H_0 = 71 \text{ km s}^{-1} \text{ Mpc}^{-1}$, $\Omega_\Lambda = 0.7$, $\Omega_M = 0.3$.

1.2 Objective of the Thesis

Our knowledge about the universe is growing day by day. But there are still many phenomena that can not be understood yet. In this circumstances, galaxy clusters, as the biggest organised structures in the universe, turn into excellent samples for studying. These kind of studies may lead us to understand the fundamental principles of cosmos. Objective of this thesis is trying to understand the properties of galaxy clusters by examining the ICM. X-ray observations gives the essential information about these properties of clusters. With this motivation, we analyse the x-ray observation data taken from the x-ray observatories and search for answers that can make contribution to our understanding.

1.3 Hypothesis

With the influence of our objective, we decided to study galaxy cluster Abell 2554. Among the unstudied cluster observations, A2554 seemed suitable for our research, due to some signatures that A2554 is part of an ongoing merger. We can observe the inner dynamics of merging clusters better, because the merging event triggers this dynamics. In this work, we will present the results of detailed analysis of A2554. We will discuss the signatures and effects of merger process along with the general properties of A2554. Our discussion is going to focus mostly on morphological distortions and merger shock that we claim to exist in A2554. We also detected a possible cold front. Although some results of our analysis support this hypothesis, we couldn't find strong evidences. The observation data is insufficient for confirmation. Deeper observations may provide better results.

CHANDRA OBSERVATORY

2.1 General Information



Figure 2.1 Chandra X-ray Observatory (CXO)

The Chandra X-ray Observatory (CXO), previously known as the Advanced X-ray Astrophysics Facility (AXAF), is a space observatory launched on STS-93 by NASA on July 23, 1999. Chandra is sensitive to X-ray sources 100 times fainter than any previous X-ray telescope, enabled by the high angular resolution of its mirrors. Since the Earth's atmosphere absorbs the vast majority of X-rays, they are not detectable from Earth-based telescopes; therefore space-based telescopes are required to make these observations. Chandra is an Earth satellite in a 64-hour orbit, and its mission is ongoing as of 2016. The telescope is named after astrophysicist Subrahmanyan Chandrasekhar.

2.2 Technical Description

Unlike optical telescopes which possess simple aluminized parabolic surfaces (mirrors), X-ray telescopes generally use a Wolter telescope consisting of nested cylindrical paraboloid and hyperboloid surfaces coated with iridium or gold. X-ray photons would be absorbed by normal mirror surfaces, so mirrors with a low grazing angle are necessary to reflect them. Chandra uses four pairs of nested mirrors, together with their support structure, called the High Resolution Mirror Assembly (HRMA); the mirror substrate is 2 cm-thick glass, with the reflecting surface a 33 nm iridium coating, and the diameters are 65 cm, 87 cm, 99 cm and 123 cm. The thick substrate and particularly careful polishing allowed a very precise optical surface, which is responsible for Chandra's unmatched resolution: between 80% and 95% of the incoming X-ray energy is focused into a one-arcsecond circle. However, the thickness of the substrates limit the proportion of the aperture which is filled, leading to the low collecting area compared to XMM-Newton.

Chandra's highly elliptical orbit allows it to observe continuously for up to 55 hours of its 65-hour orbital period. At its furthest orbital point from Earth, Chandra is one of the most distant Earth-orbiting satellites. This orbit takes it beyond the geostationary satellites and beyond the outer Van Allen belt.

With an angular resolution of 0.5 arcsecond ($2.4 \mu\text{rad}$), Chandra possesses a resolution over 1000 times better than that of the first orbiting X-ray telescope.

2.3 Instruments

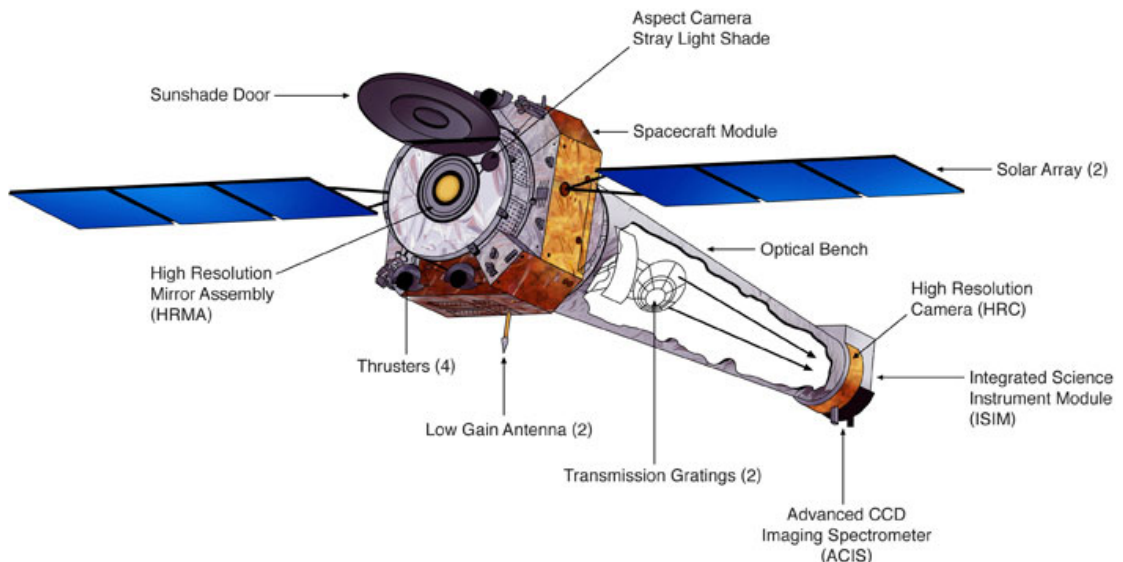


Figure 2.2 CXO Instruments

The Chandra X-Ray Observatory combines the mirrors with four science instruments to capture and probe the X-rays from astronomical sources. The incoming X-rays are focused by the mirrors to a tiny spot (about half as wide as a human hair) on the focal plane, about 30 feet away. The focal plane science instruments, ACIS and HRC, are well matched to capture the sharp images formed by the mirrors and to provide information about the incoming X-rays: their number, position, energy and time of arrival.

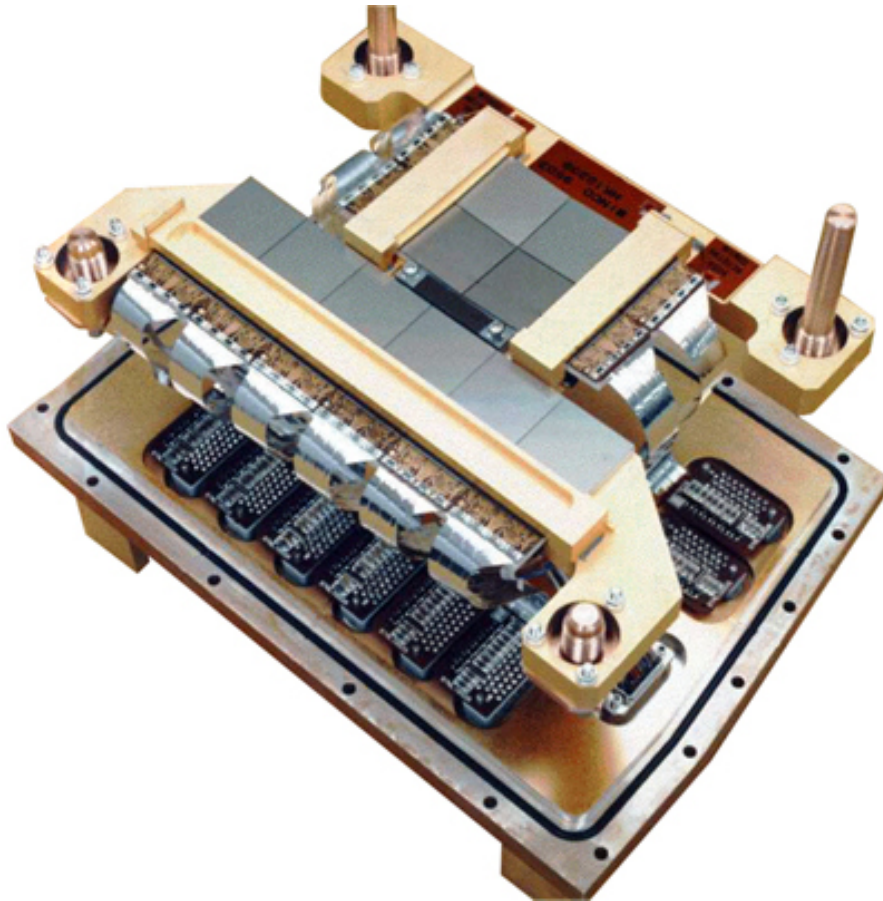


Figure 2.3 Advanced CCD Imaging Spectrometer (ACIS)

Two additional science instruments provide detailed information about the X-ray energy, the LETG and HETG spectrometers. These are grating arrays which can be flipped into the path of the X-rays just behind the mirrors, where they redirect (diffract) the X-rays according to their energy. The X-ray position is measured by HRC or ACIS, so that the exact energy can be determined. The science instruments have complementary capabilities to record and analyze X-ray images of celestial objects and probe their physical conditions with unprecedented accuracy.

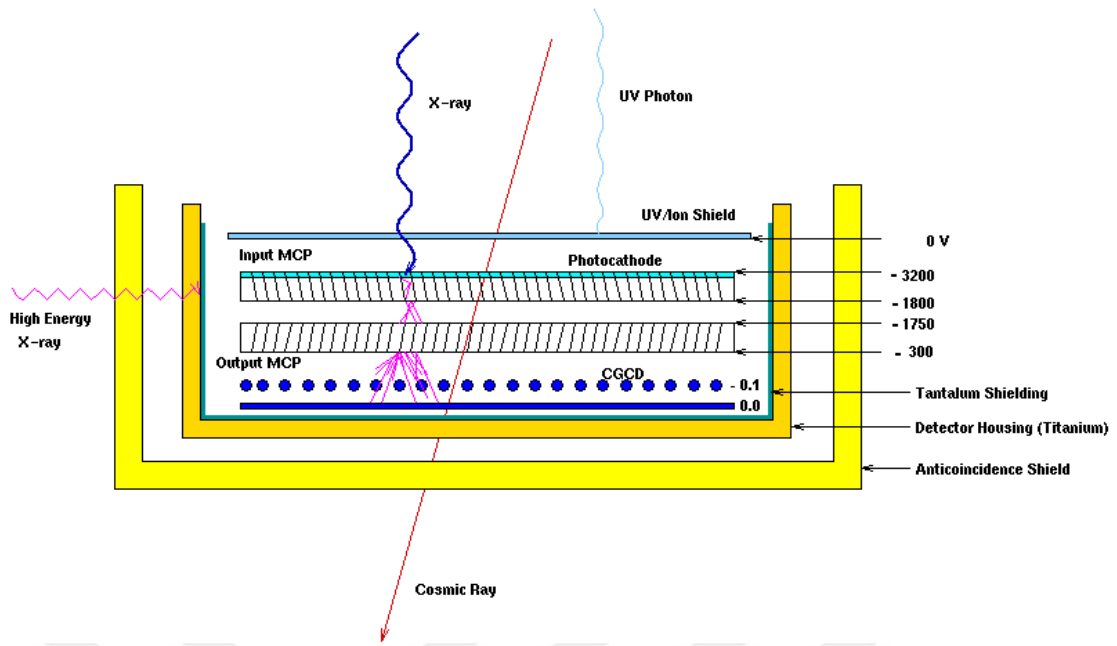


Figure 2.4 High Resolution Camera (HRC) Illustration

The High Resolution Camera (HRC) is one of two instruments used at the focus of Chandra, where it detects X-rays reflected from an assembly of eight mirrors. The unique capabilities of the HRC stem from the close match of its imaging capability to the focusing power of the mirrors. When used with the Chandra mirrors, the HRC can make images that reveal detail as small as one-half an arc second. This is equivalent to the ability to read a newspaper at a distance of half a mile.

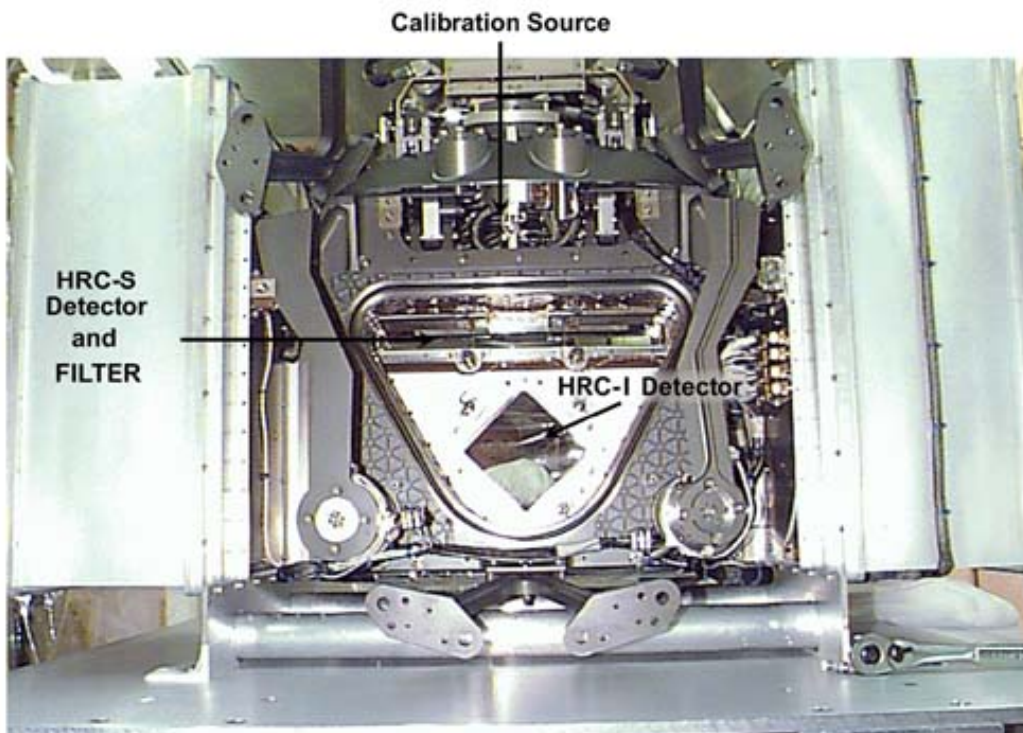


Figure 2.5 HRC

The primary components of the HRC are two Micro-Channel Plates (MCP). They each consist of a 10-cm (4-inch) square cluster of 69 million tiny lead-oxide glass tubes that are about 10 micrometers in diameter (1/8 the thickness of a human hair) and 1.2 millimeters (1/20 an inch) long. The tubes have a special coating that causes electrons to be released when the tubes are struck by X-rays. These electrons are accelerated down the tube by a high voltage, releasing more electrons as they bounce off the sides of the tube. By the time they leave the end of the tube, they have created a cloud of thirty million electrons. A crossed grid of wires detects this electronic signal and allows the position of the original X-ray to be determined with high precision. With this information astronomers can construct a finely detailed map of a cosmic X-ray source. The (HRC) is especially useful for imaging hot matter in remnants of exploded stars, and in distant galaxies and clusters of galaxies, and for identifying very faint sources.

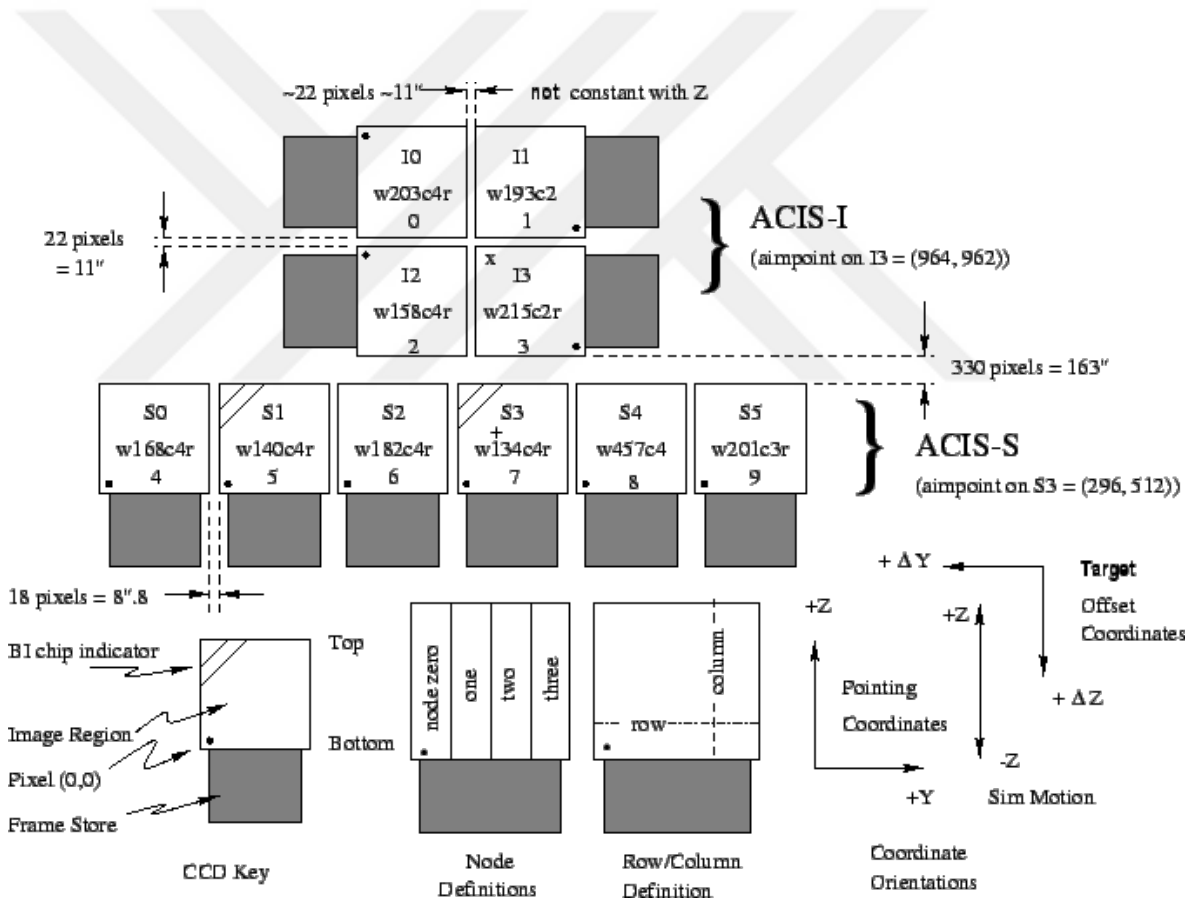


Figure 2.6 ACIS

The Chandra Advanced CCD Imaging Spectrometer (ACIS) is one of two focal plane instruments. As the name suggests, this instrument is an array of charged coupled devices (CCD's), which are sophisticated versions of the crude CCD's used in camcorders. This instrument is especially useful because it can make X-ray images, and at the same time, measure the energy of each incoming X-ray. Thus

scientists can make pictures of objects using only X-rays produced by a single chemical element, and so compare (for example) the appearance of a supernova remnant in light produced by oxygen ions to that of neon or iron ions. It is the instrument of choice for studying temperature variations across X-ray sources such as vast clouds of hot gas in intergalactic space, or chemical variations across clouds left by supernova explosions.

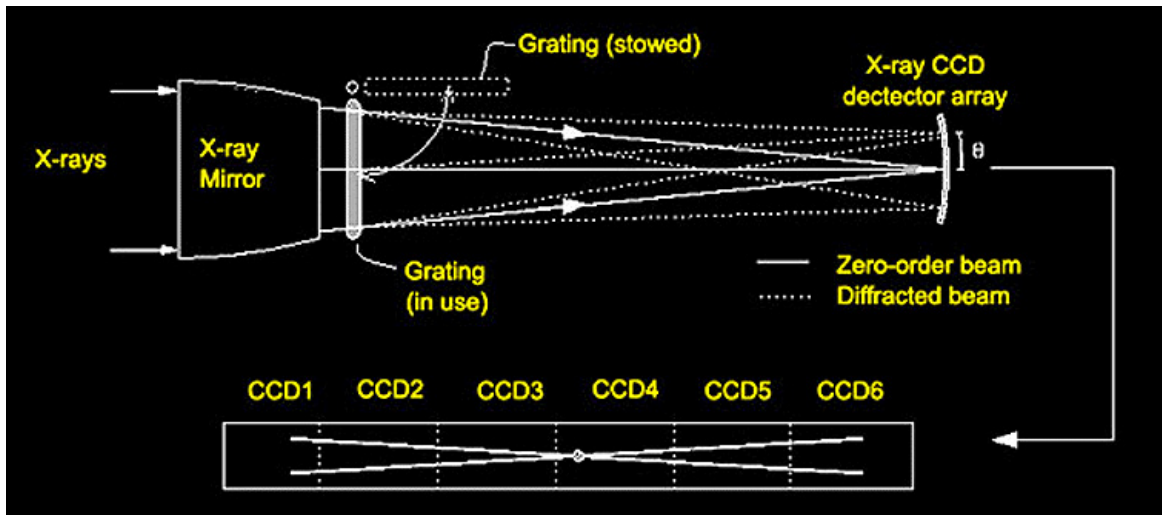


Figure 2.7 Transmission Gratings

There are two instruments aboard Chandra dedicated to high resolution spectroscopy: the High Energy Transmission Grating Spectrometer (HETGS) and the Low Energy Transmission Grating Spectrometer (LETGs). Each spectrometer is activated by swinging an assembly into position behind the mirrors. The assembly holds hundreds of gold transmission gratings: when in place behind the mirrors, the gratings intercept the X-rays reflected from the mirrors.

These gratings diffract the intercepted X-rays, changing their direction by amounts that depend sensitively on the X-ray energy, much like a prism separates light into its component colors. One of the focal plane cameras, either HRC or ACIS, detects the location of the diffracted X-ray, enabling a precise determination of its energy. (A grating is able to diffract because it has a regularly spaced pattern. For example, music CDs act as a type of grating: the grooves diffract, so that when light falls on the shiny side of the CD, a rainbow effect is seen. As the CD is tilted through different angles, different colors come into view.)

The gratings exploit Chandra's sharp mirror focus and matching detector resolution to produce *high resolution* X-ray spectroscopy. Since the grating spectrometers can measure energy to an accuracy of up to one part in a thousand, they are used in the study of detailed energy spectra, distinguishing individual X-ray lines. This enables the temperature, ionization and chemical composition to be explored.

The LETG grating is a freestanding gold grating made of fine wires or bars with a regular spacing, or *period*, of $1\mu\text{m}$. The fine gold wires are held by two different support structures, a linear grid with $25.4\mu\text{m}$ and a coarse triangular mesh with 2 mm spacing. The gratings are mounted onto a toroidal ring structure matched to the Chandra mirrors. The LETG gratings are designed to cover an energy range of 0.08 to 2 keV . However, their diffraction can also be seen in visible light, which is beautifully shown in the picture above right.

The HETG gratings have a much finer period, $0.2\mu\text{m}$ or 2000\AA for the high-energy gratings, and $0.4\mu\text{m}$ or 4000\AA , for the medium energy gratings. In order to distinguish between them, the two types of gratings are oriented at slightly different angles, so that the X-rays are diffracted in an "X" pattern at the focal plane. Since the size of the gold grating bars is *smaller* than a wavelength of visible light, special fabrication techniques are required to make them. The gratings take advantage of the fact that the gold bars are partially transparent to X-rays, so that the diffraction is more efficient, and more X-rays are captured in the high resolution spectrum. The HETG gratings are designed to cover an energy range of 0.4 to 10 keV .

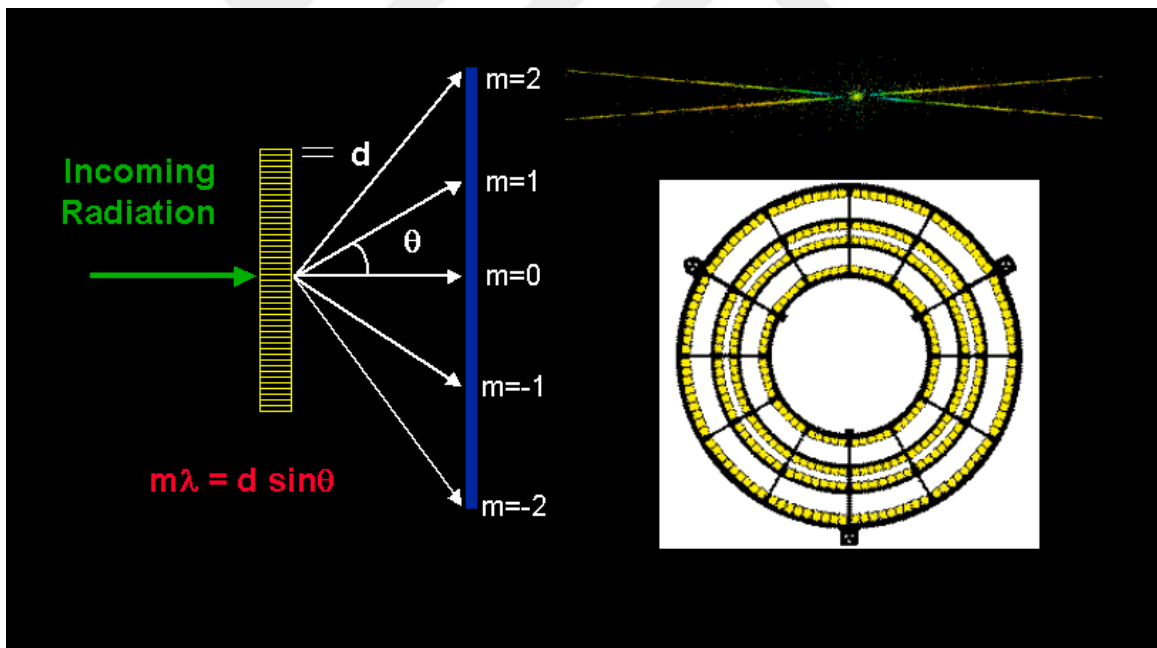


Figure 2.8 Chandra Grating Spectrometers

The focal plane instruments are mounted on the Science Instrument Module (SIM). The SIM contains mechanisms to move the science instruments in and out of the focal plane, insulation for thermal control, and electronics to control the operation of the science instruments via the communication, command and data management systems of the spacecraft.

The science instruments are controlled by commands transmitted from the Operations Control Center in Cambridge, Massachusetts. A preplanned sequence of observations is uplinked to Chandra and stored in the onboard computer for later execution.

Data collected by observations with Chandra are stored on a recorder for later transmission to the ground every eight hours during regularly scheduled Deep Space network contacts. The data is then transmitted to the Jet Propulsion Laboratory and then to Operations Control at the Chandra X-ray Center (CXC) in Cambridge, MA for processing and analysis by scientists.



OBSERVATION AND DATA REDUCTION

3.1 Abell 2554

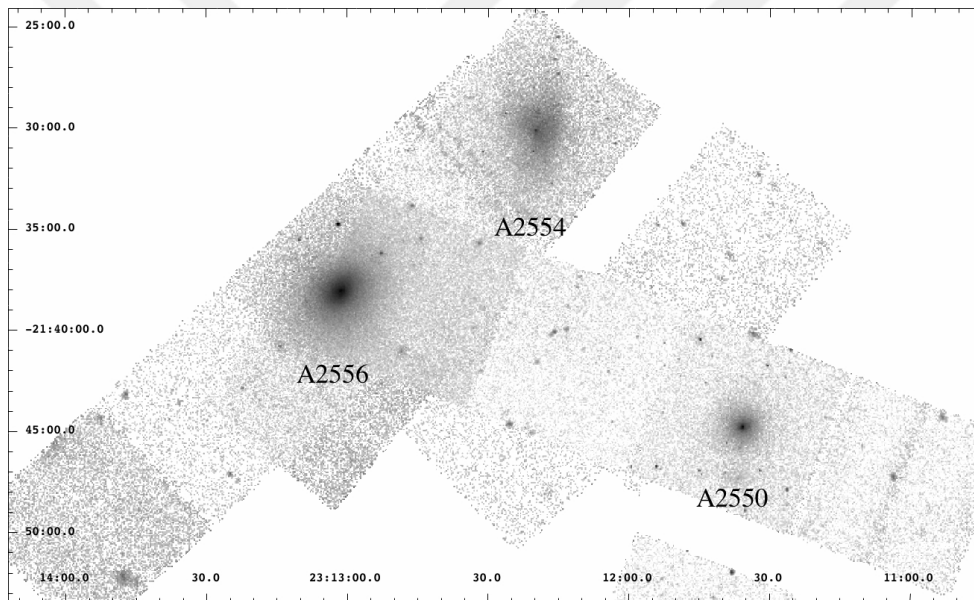


Figure 3.1 X-ray image of the trio-clusters A2550, A2554 and A2556

A2554 is a galaxy clusters with a redshift of $z=0.11$. Hydrogen column density value is $nH=2.09 \times 10^{20} \text{ cm}^{-2}$ [10]. A2554 is member of a trio-cluster system with two other clusters A2550 ($z=0.1226$) and A2556 ($z=0.0871$). Projected distances from A2554 to A2550 and A2556 are 2.07 Mpc and 1.47 Mpc, respectively. They are members of Aquarius Super Cluster [11]. Results of detailed analysis of A2554 will be presented. Our discussion is going to focus mostly on morphological distortions and merger shock that we claim to exist in A2554. We used CHANDRA observation for analysis. Detailed information about the observation is summarized in Table 3.1.

A2554 shows some signatures that the cluster is part of an ongoing merger. We can observe the inner dynamics of merging clusters better, because the merging event triggers this dynamics. This makes A2554 suitable for our work.

Table 3.1 Information about galaxy cluster A2554

Object name	Abell 2554
Coordinates (J2000)	R.A: 23 12 19.3 DEC: -21 29 52.4
Redshift (z)	0.11
Column Density (nH)	$2.09 \times 10^{20} \text{ cm}^{-2}$
Observatory	Chandra
Observation ID	1696
Observation Date	21-10-2001
Exposure Time	20140 s
Detector	ACIS-S

Assuming the Hubble Constant $H_0 = 71 \text{ km s}^{-1} \text{ Mpc}^{-1}$, angular size distance for A2554 is 408 Mpc and angular size of 1 arc-sec corresponds to 1.978 kpc. The software used for analyze are HEASOFT v1.16, CIAO v4.7 with CALDB v4.6.7. and XSPEC v12.8.2.

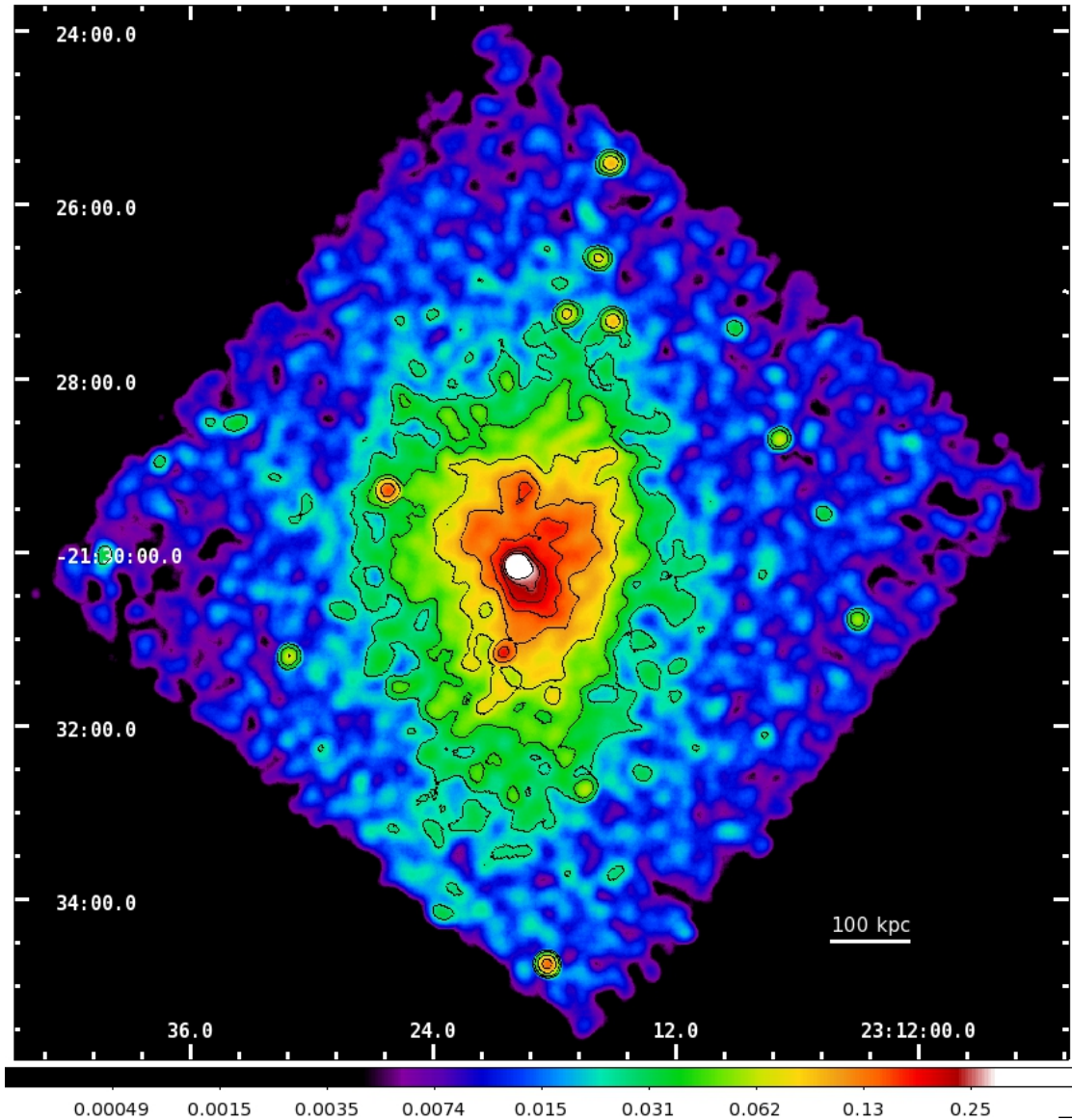


Figure 3.2 X-ray image of A2554

3.2 Data Reduction

We used the “*chandra_repro*” reprocessing script to create level=2 event file. The S3 chip of ACIS-S array was used for analyze and filtered between 0.5 keV - 7.0 keV energy range. Background flares were cleaned with “*dmextract*” tool. Total exposure time is decreased to 19.8 ks from 20.1 ks after cleaning. We used “*SAOImage ds9*” software to display images. Background and exposure corrected images were created for the cluster (Figure 3.2). Point sources were detected with “*wavdetect*” tool and filtered to analyze intra-cluster medium (ICM). Filtered image of the cluster is shown in Figure 4.1.

After source cleaning, we extracted the spectrum of the cluster for selected regions. These regions were showed in Figure 4.9 with an additional region used for background. “*specextract*” tool was used to create ARF, RMF, background and “*grp*” files for each region. These files were modeled and fitted for overall region and 10 sub-regions with XSPEC using an absorbed single temperature model (APEC) (Smith et al. 2001) [12] to calculate plasma temperatures, abundances and normalizations. Hydrogen column density (nH) values were fixed for each region. Temperature, abundance and normalization values were set free. Average values and the radial distribution for plasma temperatures and abundances of cluster are shown in Figure 4.11.



4.1 Overview

In this chapter, analysis methods are presented.

4.1.1 X-ray Images of A2554

We created exposure corrected x-ray images of the cluster between energy ranges of 0.5–1.35 keV (soft band), 1.35–7.0 keV (hard band) and 0.5–7.0 keV (all band). Images of optic and radio observations were also taken from the SAO-DSS and NRAO-NVSS. They will be discussed later. All the calculations are made according to projected values. Confidence level of the calculated values is 90%.

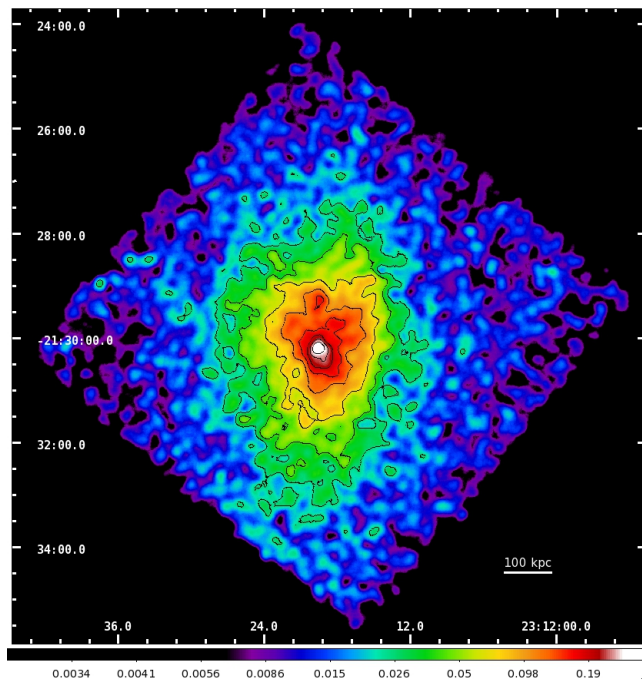


Figure 4.1 All band x-ray image of A2554 (filtered)

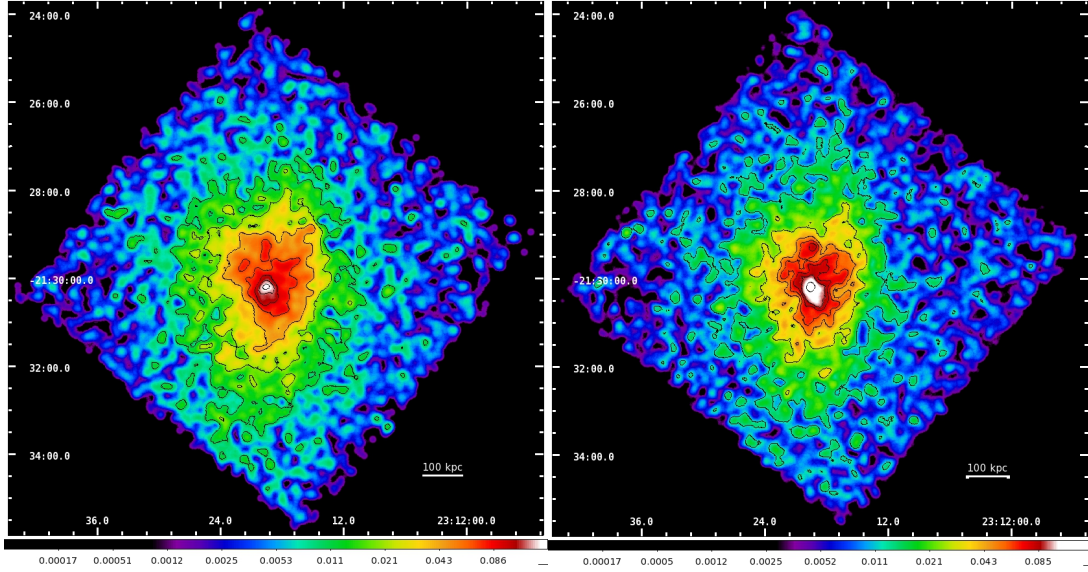


Figure 4.2 Soft x-ray image (left), hard x-ray image (right) of A2554

Figure 4.1 and Figure 4.2 shows the filtered, exposure corrected and point sources removed images of A2554. It can be seen from the images that the cluster has an elongation towards vertical axis. There is also a major distortion, located at the south east of the cluster core. Relaxed clusters are mostly has spherical morphology and symmetric distribution. The A2554 galaxy cluster is in a non-relaxed state.

4.1.2 Surface Brightness Profile

Surface brightness profile is essential to detect the disrupted regions in the ICM and see the merger signatures. It gives us information about how the brightness of the cluster changes radially. In relaxed, undisturbed clusters, profile should be continuous, since non-relaxed clusters profile has discontinuities. It is done by calculating the x-ray counts of selected region that contains annulus. Initially, we calculated the surface brightness profile for a circular region with 55 annuli, starting from the center of the cluster. Then we split the selected region into 3 pieces to see the profile in detail. We applied the king model to profiles in order to calculate core radius and β parameter. Although the model didn't fit well, it was what we expected from a disturbed, non-symmetric cluster. Calculated values are 57 kpc and 0.61, respectively. Selected regions and the profile for the whole cluster are shown in Figure 4.3 and Figure 4.4. Profiles for the sub-regions are shown in Figure 4.5,

Figure 4.6 and Figure 4.7. Sub-region selection was decided according to hardness ratio map, which will be discussed later. We detected discontinuities in the profiles. Discontinuities and their locations on x-ray image will be discussed in Chapter 5.

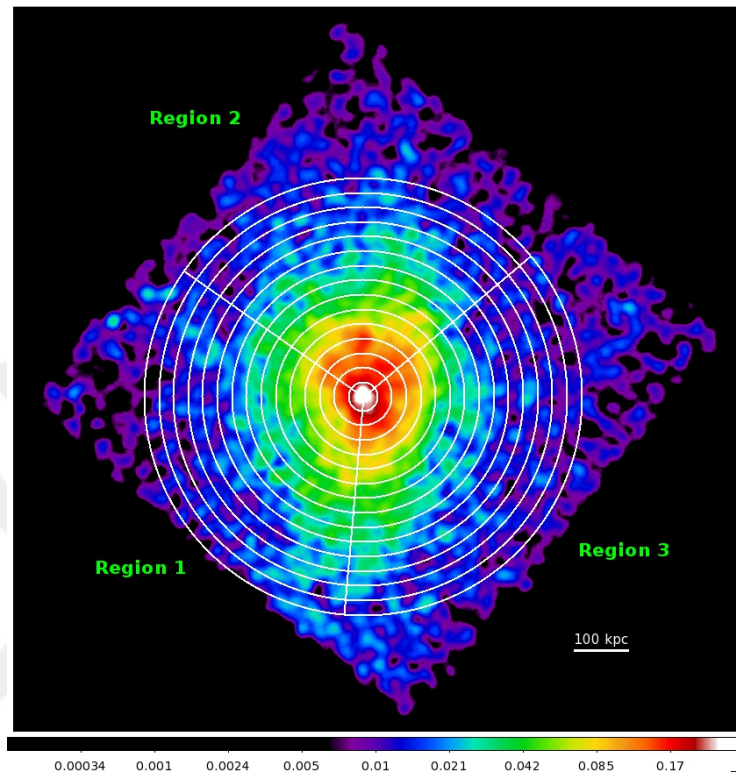


Figure 4.3 Selected regions for surface brightness profile

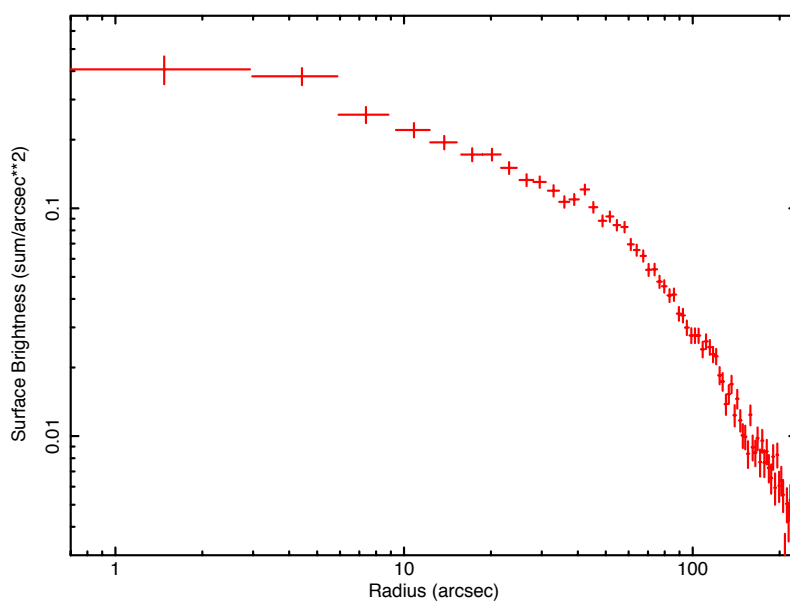


Figure 4.4 Surface brightness profile (whole cluster)

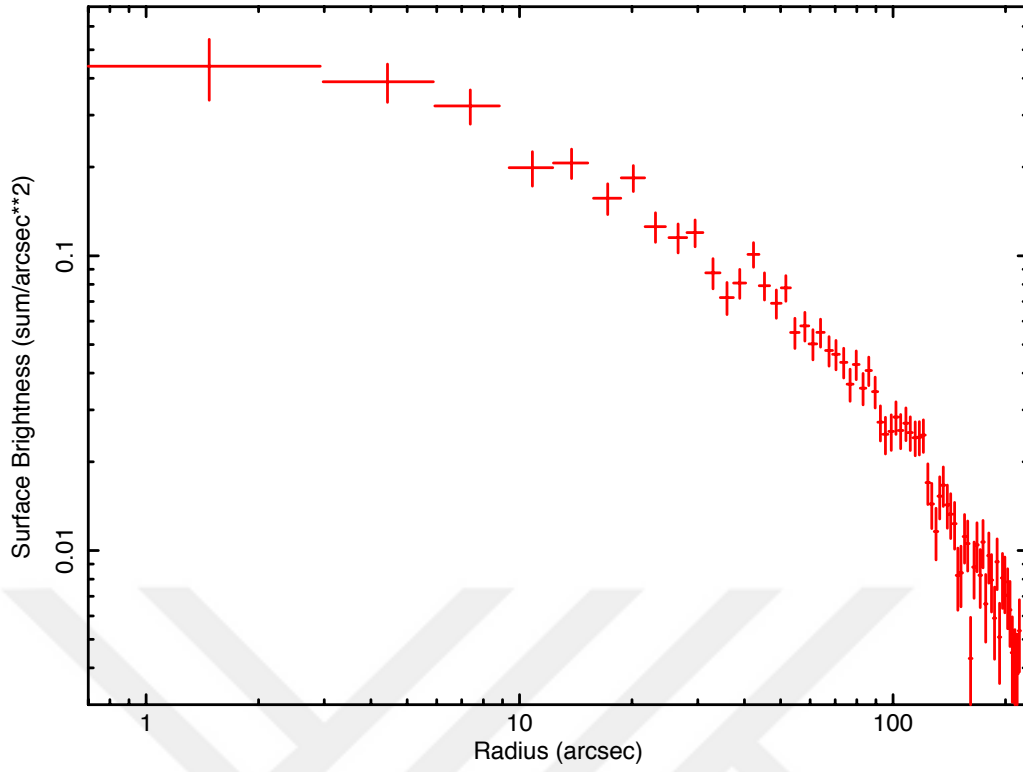


Figure 4.5 Surface brightness profile (region 1)

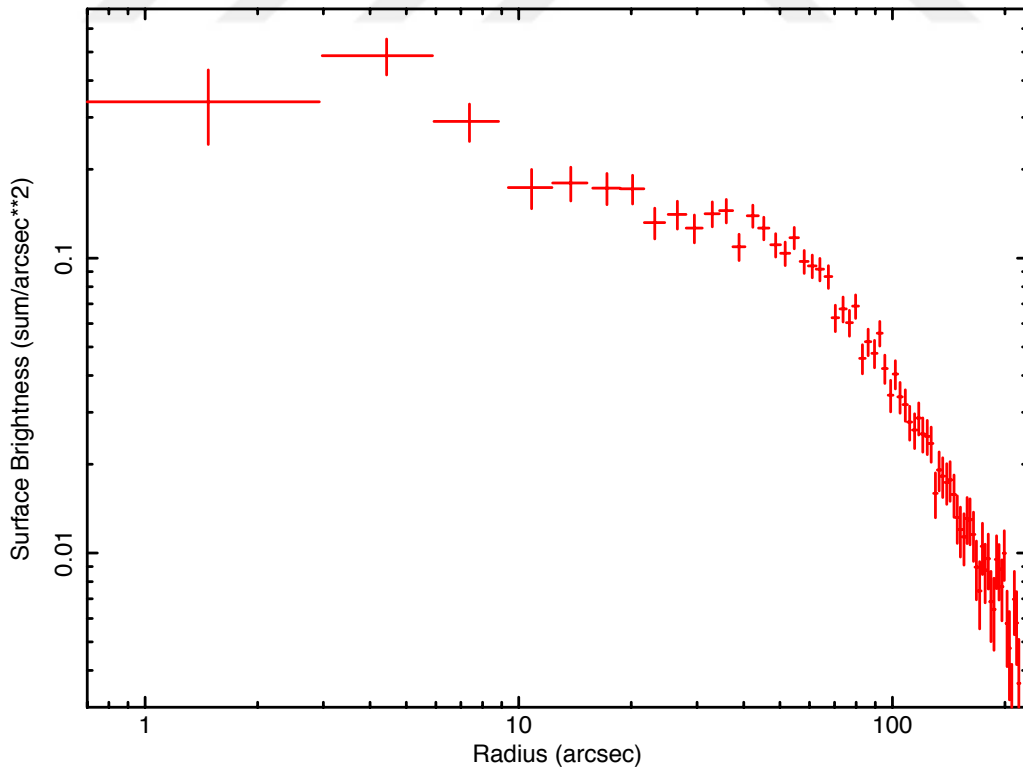


Figure 4.6 Surface brightness profile (region 2)

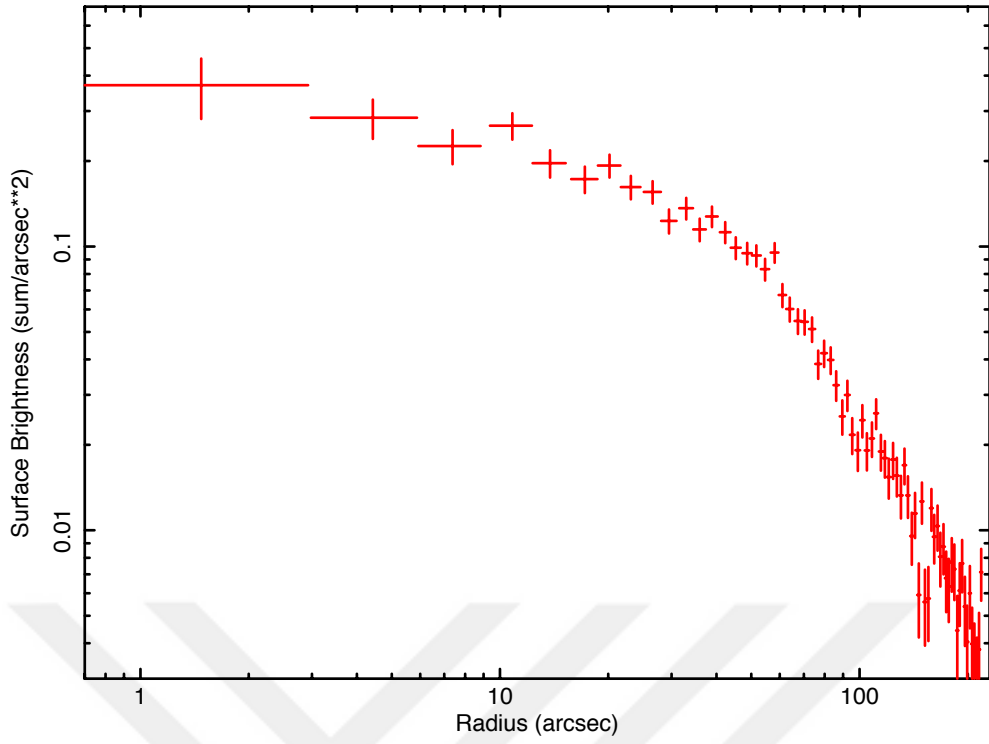


Figure 4.7 Surface brightness profile (region 3)

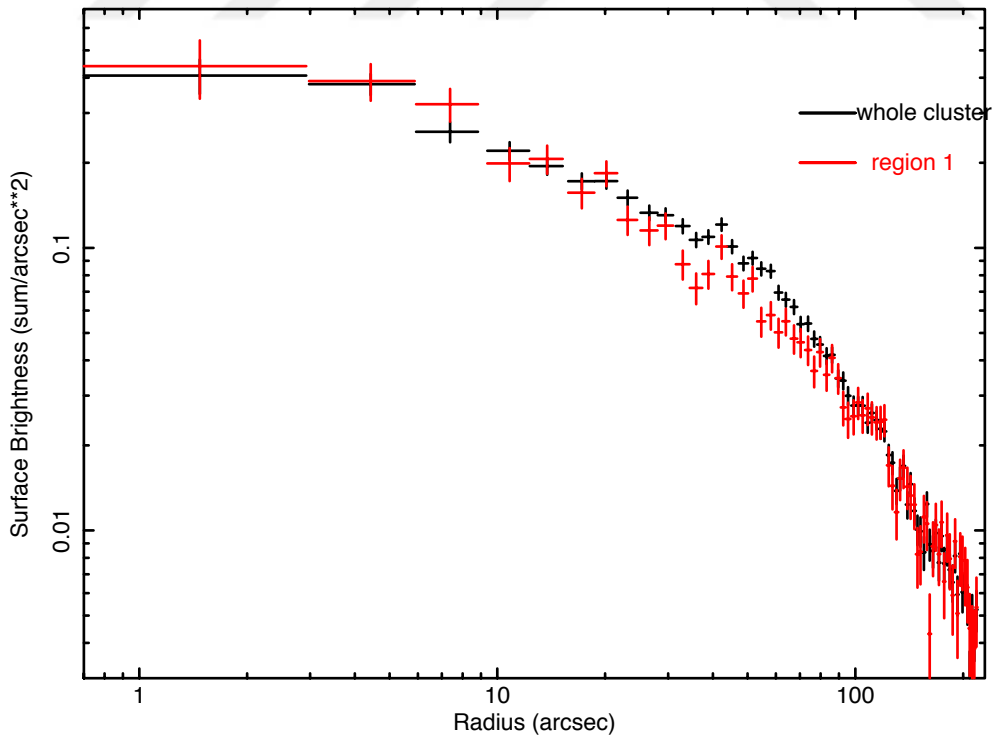


Figure 4.8 Surface brightness profile (whole cluster & region 1)

4.2 Spectral Analysis

First we selected a circular region that covers the cluster with a 2.5 arcmin radius, centered on the x-ray peak. Then we extracted the spectrum of the region and calculated the average temperature and abundance using XSPEC. Absorbed single temperature model (APEC) [12] is used to fit the data. In order to see the radial distributions of temperature and abundance, we divided the initially selected region into 10 sub-regions and extract spectrum from each of them. We fitted the sub-regions with the same steps. Results of the spectral analysis are showed in the Figure 4.10, Figure 4.11 and Table 4.1. Black lines in the Figure 4.11 shows the average temperature value of the cluster, which is calculated by analyzing the region in Figure 4.9 (left). Figure 4.11 shows the spectrum of the same region between 0.5-7.0 keV energy range with residuals (lower panel). It is calculated from the spectral analysis that 1.35 keV is the energy value that splits the total counts of the cluster equally, between 0.5 keV - 7 keV energy range. We made the soft-hard energy range separation according to this. Chi-squared method is selected for obtaining statistical values.

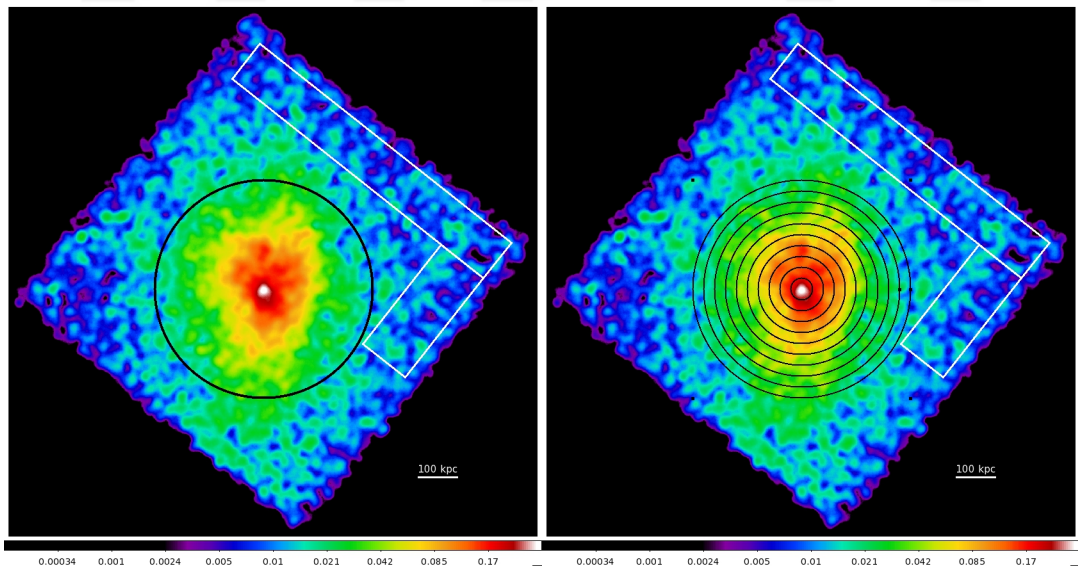


Figure 4.9 The regions used for spectrum extraction (black) and the selected background region (white)

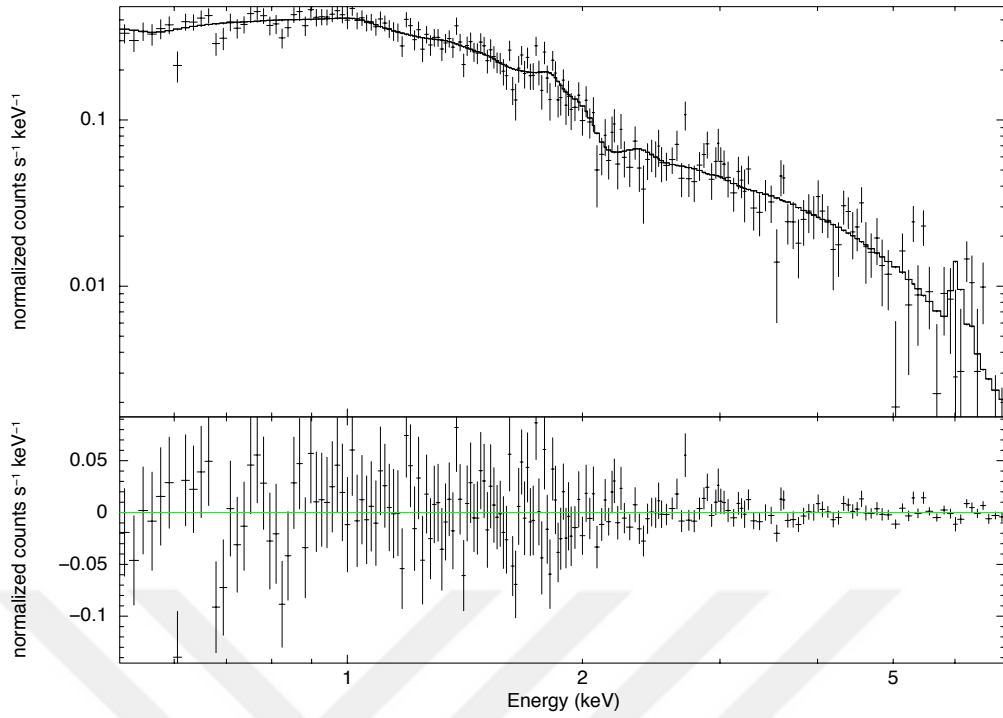


Figure 4.10 Spectrum of A2554

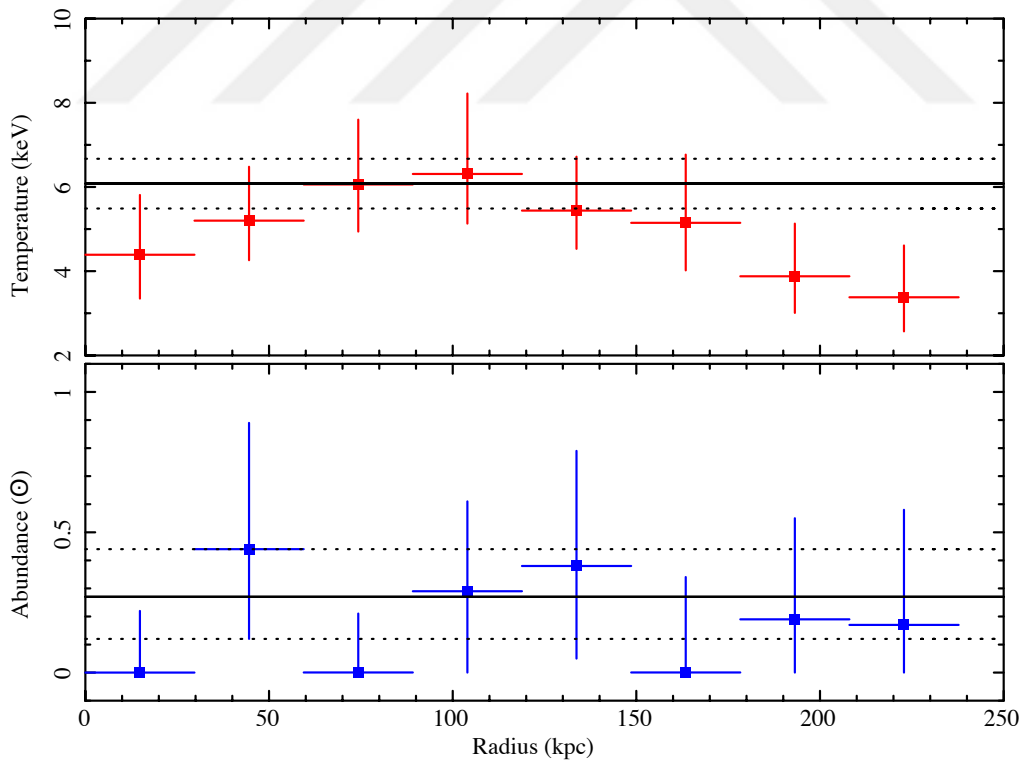


Figure 4.11 Radial temperature distribution

Table 4.1 Spectral values for analyzed regions

	kT_e (keV)	Abundance (Z_\odot)	χ^2/dof
0''-15''	4.39 ^{+1.42} _{-1.04}	0.00 ^{+0.22} _{-0.00}	126/157 = 0.80
15''-30''	5.20 ^{+1.28} _{-0.94}	0.44 ^{+0.45} _{-0.32}	145/169 = 0.86
30''-45''	6.06 ^{+1.54} _{-1.12}	0.00 ^{+0.21} _{-0.00}	159/153 = 1.04
45''-60''	6.31 ^{+1.91} _{-1.18}	0.29 ^{+0.32} _{-0.29}	153/156 = 0.98
60''-75''	5.44 ^{+1.28} _{-0.91}	0.38 ^{+0.41} _{-0.33}	143/146 = 0.98
75''-90''	5.15 ^{+1.62} _{-1.13}	0.00 ^{+0.34} _{-0.00}	128/154 = 0.83
90''-105''	3.88 ^{+1.25} _{-0.87}	0.19 ^{+0.36} _{-0.19}	146/142 = 1.03
105''-120''	3.38 ^{+1.23} _{-0.81}	0.17 ^{+0.41} _{-0.17}	149/160 = 0.93
120''-135''	3.95 ^{+1.48} _{-1.08}	0.57 ^{+0.93} _{-0.46}	154/172 = 0.89
135''-150''	2.98 ^{+1.60} _{-0.84}	0.06 ^{+0.33} _{-0.06}	112/133 = 0.84
0''-150''	6.13 ^{+0.58} _{-0.59}	0.28 ^{+0.17} _{-0.15}	283/262 = 1.08

4.3 Hardness-Ratio Map

The exposure corrected soft and hard band images that created from the filtered event file with the energy ranges of 0.5 keV - 1.35 keV (soft) and 1.35 keV - 7 keV (hard) are used to create hardness-ratio map. 1.35 keV is the energy value that splits the total counts of the cluster equally, between 0.5 keV - 7 keV energy range. We smoothed both images with “*csmooth*” tool (sigma min=3, sigma max=4) and divided them with “*dmimgcalc*” tool to obtain HARD/SOFT ratio (Figure 4.12).

Hardness-ratio (HR) map of a cluster gives information about the temperature distribution of the ICM. Harder regions are expected to be hotter than the softer regions. Hard and soft regions can be detected from the image. HR map in Figure 4.12 indicates that the plasma of the cluster is turbulent. There is a hard, wall-like structure located at the south-western side of the center. This region can be seen in the x-ray image as a distortion. There is also a soft, circular shaped region next to the wall. These regions have sharply changed HR values comparing their neighbor areas, and will be analyzed in detail.

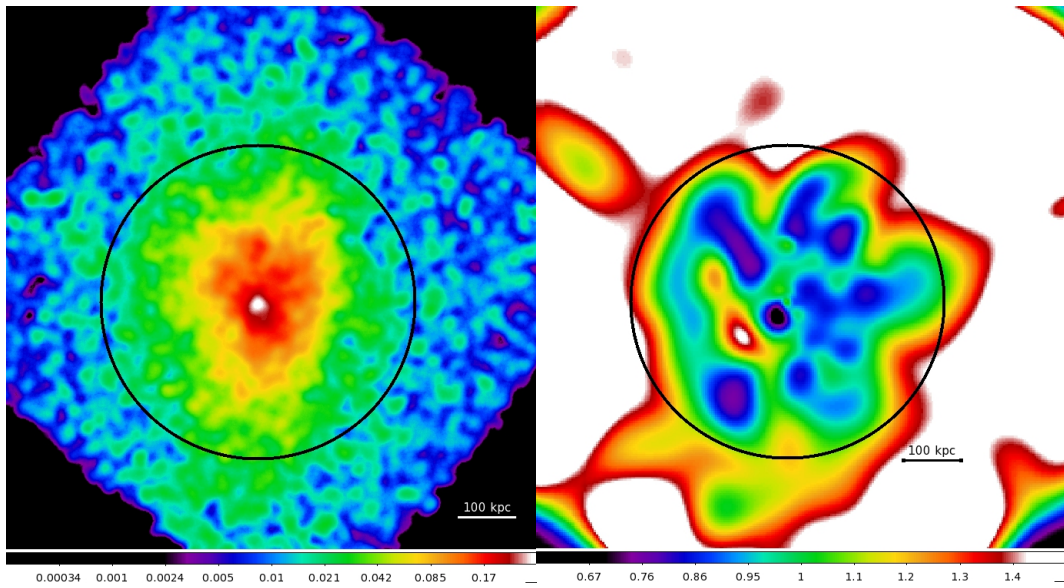


Figure 4.12 X-ray image (left) and hardness-ratio map (right) of A2554

4.4 Temperature Map

Before obtaining temperature map, some arbitrary regions are selected and analyzed to be sure that the hardness-ratio map gives the expected temperature distribution. This regions and their temperature values are shown in the Figure 4.13 and Figure 4.14.

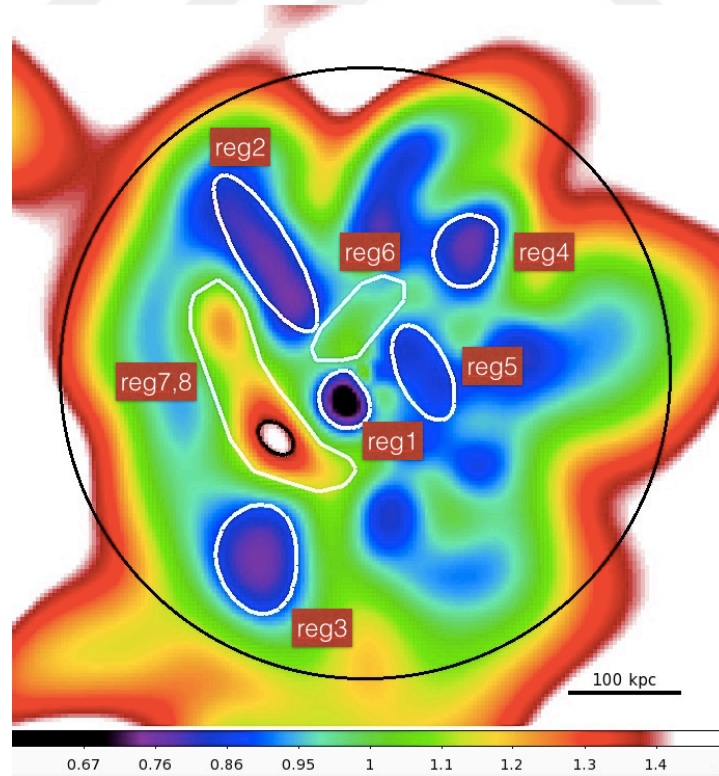


Figure 4.13 Selected regions for confirmation of the hardness-ratio/temperature relation

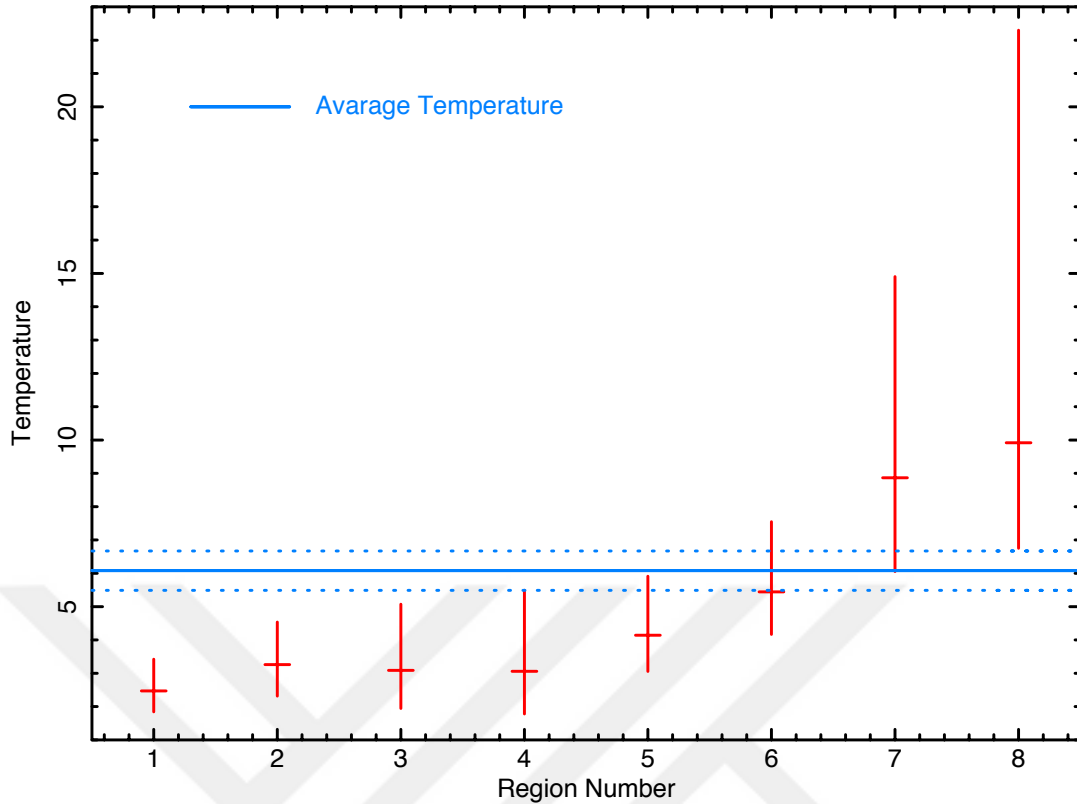


Figure 4.14 Temperature values of the regions in Figure 4.13

The black region has very low counts to extract spectrum from it. So we split the last region into two parts to see the contribution of the hardest region. In region 7, the black colored region is excluded. In region 8, it is not. As we see from Figure 4.14, results are consistent with our expectation. Harder regions in the HR map have higher temperature than softer regions.

As long as we confirmed that the HR values are related with temperature values, now we can create a temperature map. We calculated the temperature values of the regions that correspond to specific HR interval to identify the factor between HR and temperature (e.g., temperature value of the region that covers 1.0-1.2 HR interval). Selected HR intervals and their temperature values are showed in Figure 4.15. We used this relation to calculate a convergence factor as an exponential function and applied it to the HR map in order to create a temperature map. (Figure 4.16)

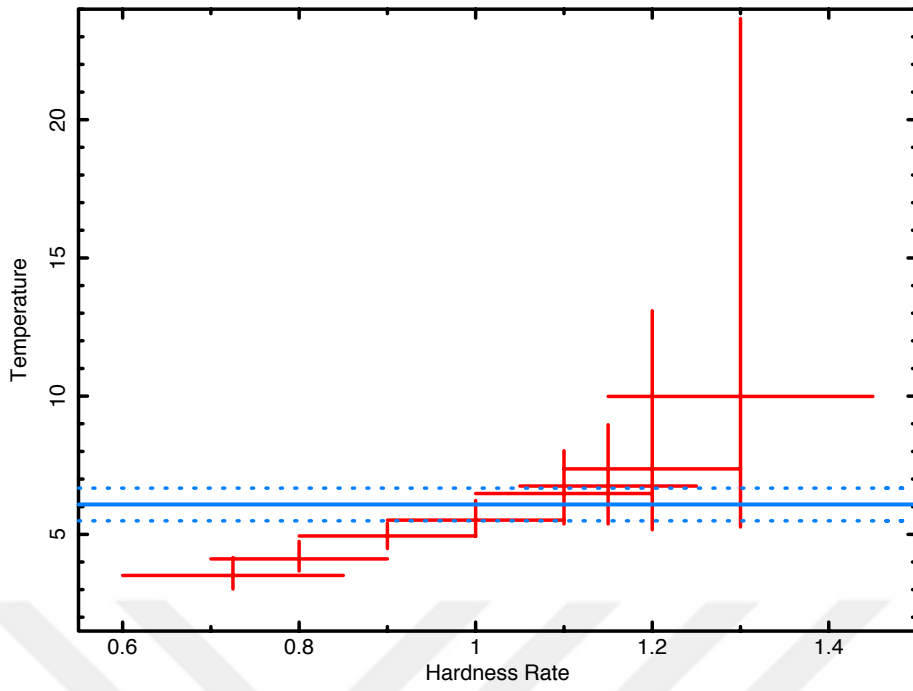


Figure 4.15 Hardness-ratio and temperature relation of A2554

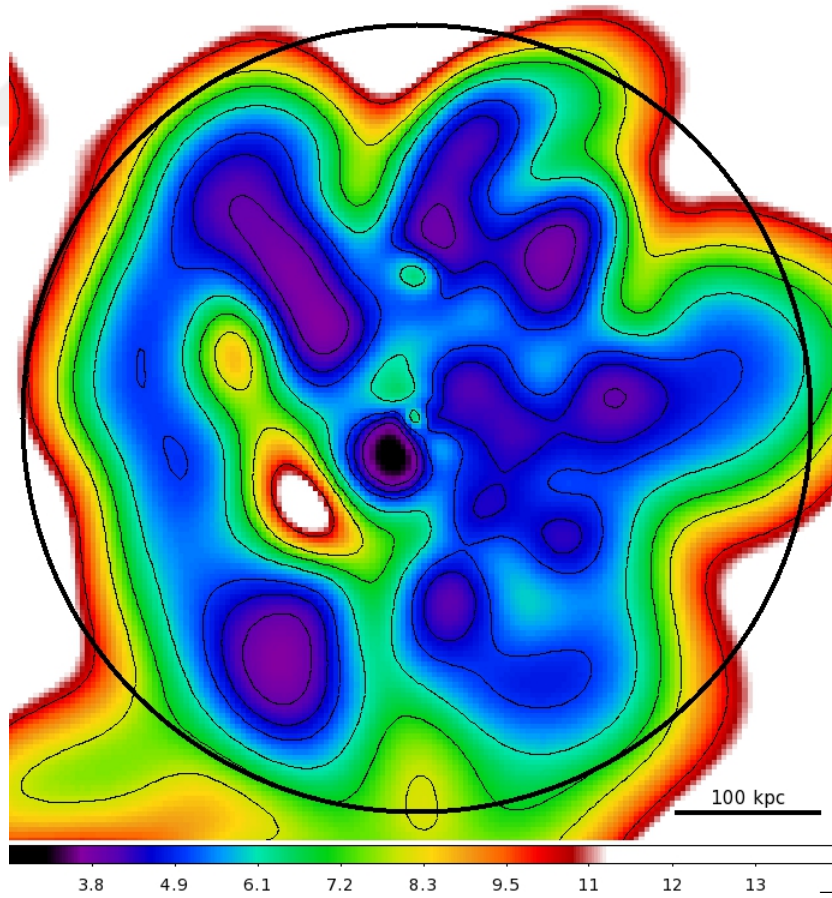


Figure 4.16 Temperature map of A2554

4.5 Pressure and Entropy Map

We prepared the pseudo pressure and entropy map by relations given in the Briel et al. [13], showed in Figure 4.17. Pseudo-pressure and pseudo-entropy maps are obtained by the relations given below. “S” is for entropy and “P” is for pressure. “I” is for soft x-ray emission. (Values of the maps are in arbitrary units.)

$$S = \frac{HR}{\sqrt[3]{I}} \quad , \quad P = HR \times \sqrt{I} \quad (4.1)$$

Pressure map show strong distortions and spiral-like distribution. Also has the same elongation as we saw in the x-ray images in previous chapters. Pressure is the maximum at the center of the cluster. A radially symmetric decrement is expected from a relaxed cluster, unlike A2554.

As we see in the entropy map, entropy distribution is also non-symmetric. The hot, wall-like structure can be detected as a high entropy area. There is a circular region near the center with the lowest entropy value which corresponds to the coldest region of the analyzed area according to temperature map. Indications of these results will be discussed in Chapter 5.

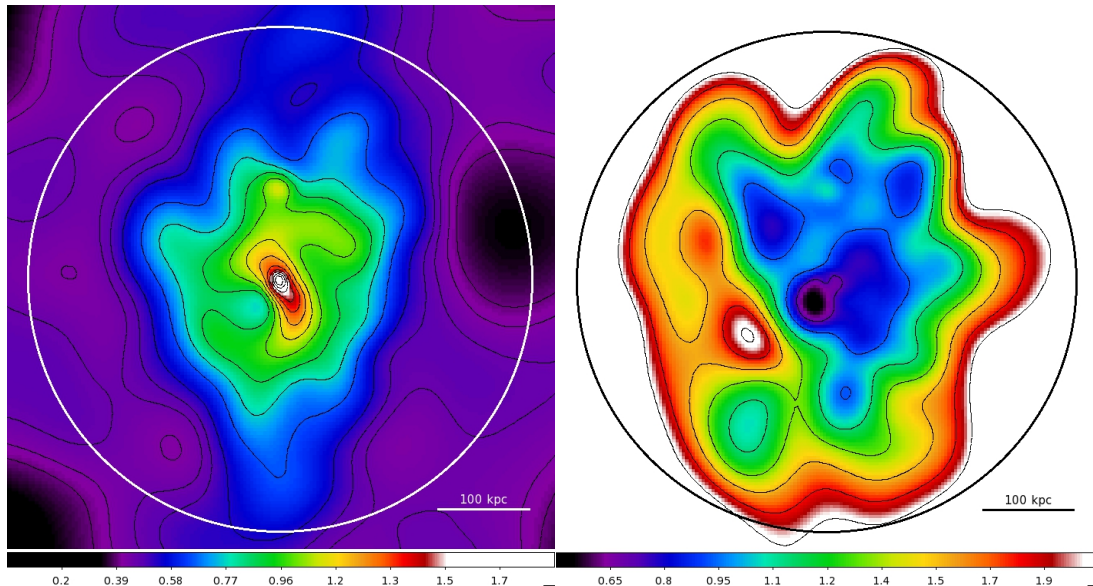


Figure 4.17 Pressure map (left) and entropy map (right) of A2554

4.6 Radio and Optic Observations

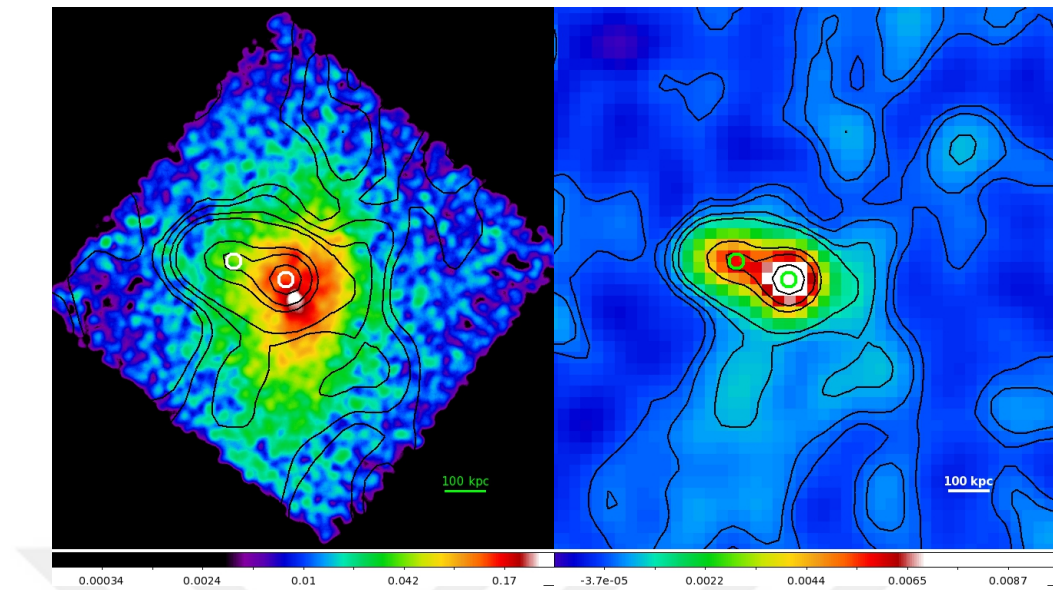


Figure 4.18 X-ray image with radio contours (left) and radio image (right) of A2554

Optic and radio images were taken from the database of SAO-DSS and NVSS, respectively. There are two radio sources with a radio emission, located on the cluster in a projected view which are located in R.A.=23:12:25.69, Dec.=-21:29:23.0 and R.A.=23:12:20.03, Dec.=-21:29:49.7 (J2000 coordinate system). Figure 4.18 shows the location of the source and the radio emission. Both optic and radio observations are unstudied for A2554.

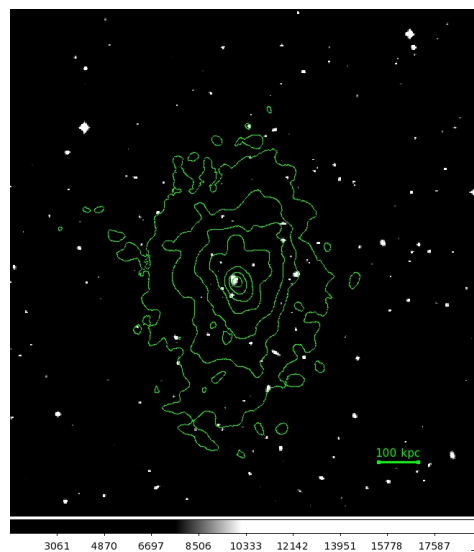


Figure 4.19 Optic image of A2554

5.1 Merger Signatures

In this chapter, results of our analysis will be discussed. Galaxy cluster A2554 has discontinuities in the surface brightness profile. This is the initial sign that the cluster is structurally disturbed. Results also show strong distortion in the temperature distribution. We can see the spiral shaped tendencies in the pressure map. These results indicates that the cluster might be in an ongoing merger. Addition to that, as we know, particle acceleration by merger shocks will produce relativistic electrons and ions, and these can produce synchrotron radio [2]. There is a radio emission located in the north-west side of the cluster. This also supports our hypothesis.

As we discussed in Chapter 4, surface brightness profile of the cluster is calculated for 4 regions. First one is a circular region that covers more than the analyzed area, with 220 kpc radius. Other 3 regions are obtained by dividing the initial region into 3 parts with different angle intervals. These regions are showed in Figure 4.3. Angle values are decided according to temperature map. Cluster has a turbulent temperature distribution. A bunch of cold gas clouds that separated by warmer boundaries and a hot, wall-like area can be seen from temperature map. Region 1 covers the hot area, which is a possible shock region. Border of the region 2 and 3 are selected according to the locations of the cold sub-regions. (We are not interested above 100 arcsec)

Figure 5.1 shows the surface brightness profile of whole cluster. We detected 4 discontinuities at ~ 6 , ~ 40 , ~ 60 , ~ 90 and ~ 120 arcsec. Figure 5.2 shows the corresponding locations on the temperature map.

Figure 5.3 shows the surface brightness profile for Region 1. First discontinuity is located at ~ 9 arcsec. Above this value, the profile shows a zigzag pattern until ~ 55 arcsec. Lastly, we see discontinuities at ~ 90 and ~ 120 arcsec. Zigzag pattern might be due to non-relaxed and highly disturbed state of the plasma. Figure 5.4 shows these regions on the temperature map.

First discontinuity corresponds to the edge of the cold circular shaped area in both profiles, with approximate values. Second one is located at the beginning of the hot region in Figure 5.2. This area is covered by the zigzagged interval of Region 1.

Third one is located near the ending of the hot region. When we combine these results with temperature map, this situation suggests that the cold, circular region and the hot, wall-like region might be originated by possible merger activity (Figure 5.5). These regions are analyzed individually. Pressure and entropy maps are used to find out their properties for better diagnose.

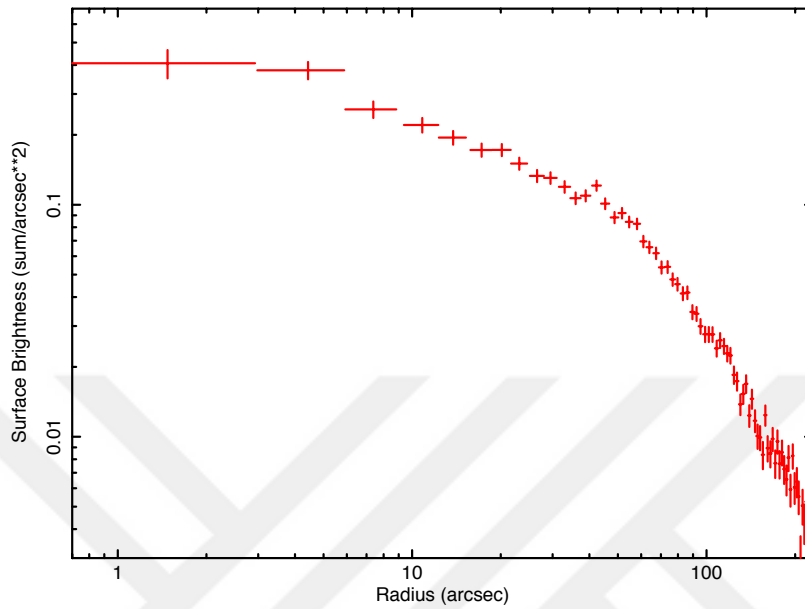


Figure 5.1 Surface brightness profile with discontinuities

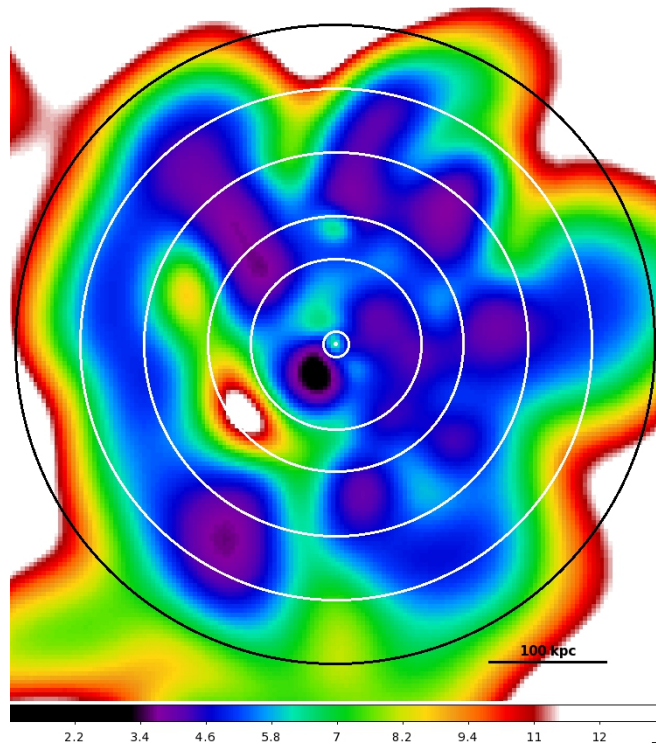


Figure 5.2 Temperature map with discontinuity regions (White colored)

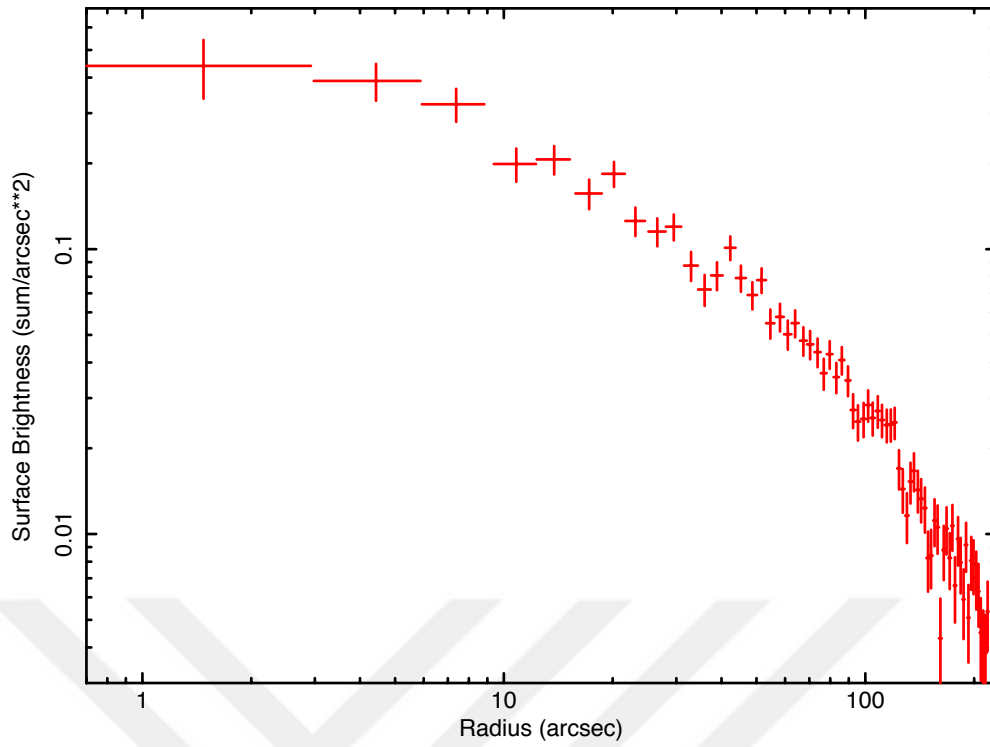


Figure 5.3 Surface brightness profile of region 1 (showed in Figure 4.3) with discontinuities

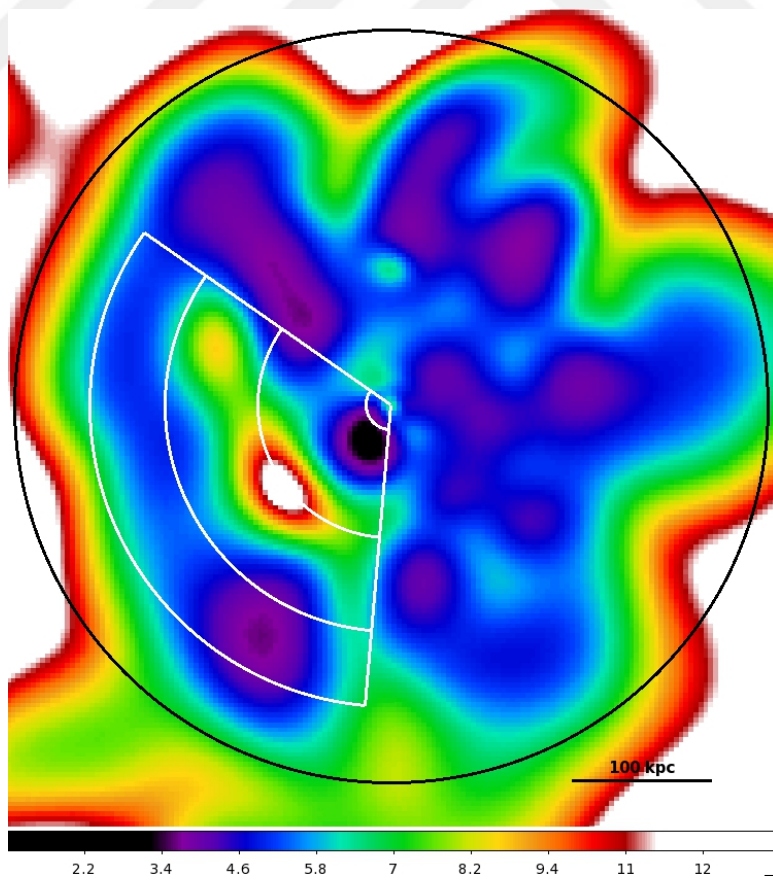


Figure 5.4 Temperature map with discontinuity regions for region 1 (White colored)

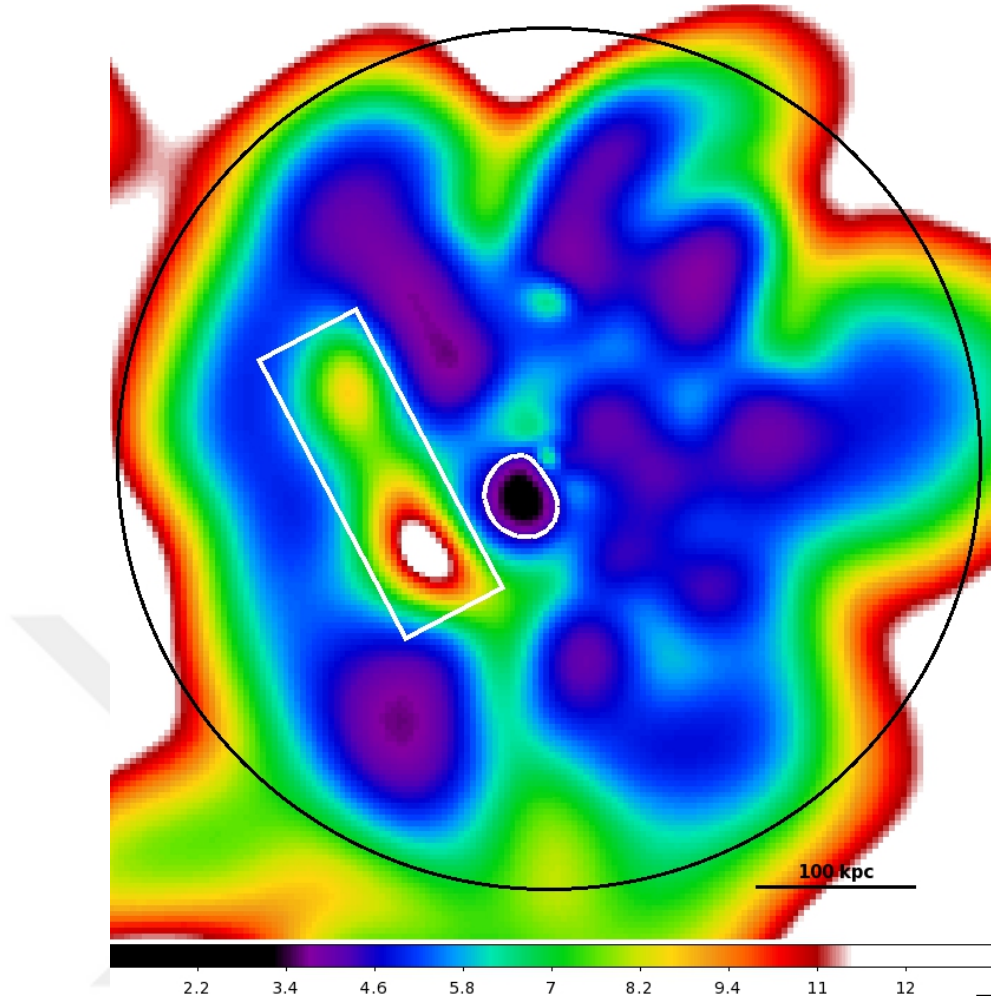


Figure 5.5 Sub-structures created by possible merger activity

5.2 Merger Shock

When we check the criterions to call a region “merger shock”, we see that the rectangle region in Figure 5.5 covers them. Merger shocks create surface brightness discontinuities as we detected in previous section. We calculated the density jump and Mach number ($M_\rho = 1.30_{-0.20}^{+0.28}$) for the possible shock region by applying Rankie-Hugoinot jump conditions [5]. Region 1 and 2 in Figure 5.6 are used for calculation. The Mach number value is also consistent with our assumption. Shocks mostly have Mach number values between 1 and 3 as indicated in Paterno-Mahler et al. [1]. ($\gamma = 5/3$ is the adiabatic index for monatomic gas)

$$M_\rho = \left[\frac{2 \frac{\rho_2}{\rho_1}}{\gamma + 1 (\gamma - 1) \frac{\rho_2}{\rho_1}} \right]^{1/2} \quad (5.1)$$

Temperature jump of the possible shock region with the pre-shock and after shock regions can be seen in Figure 5.8. We expect to see a high entropy value for the shock area. Entropy map also confirms this possibility that, merger shocks should heat and compress the x-ray emitting intra-cluster gas, and increase its entropy [2]. Pressure should change across the shock. Although there is not a sharp pressure change, if it is accepted as a “weak shock”, our pseudo-pressure map is also consistent with this criterion. It also shows the elongation and spirally shaped disturbance. Figure 5.7 shows the interested regions on pressure and entropy map.

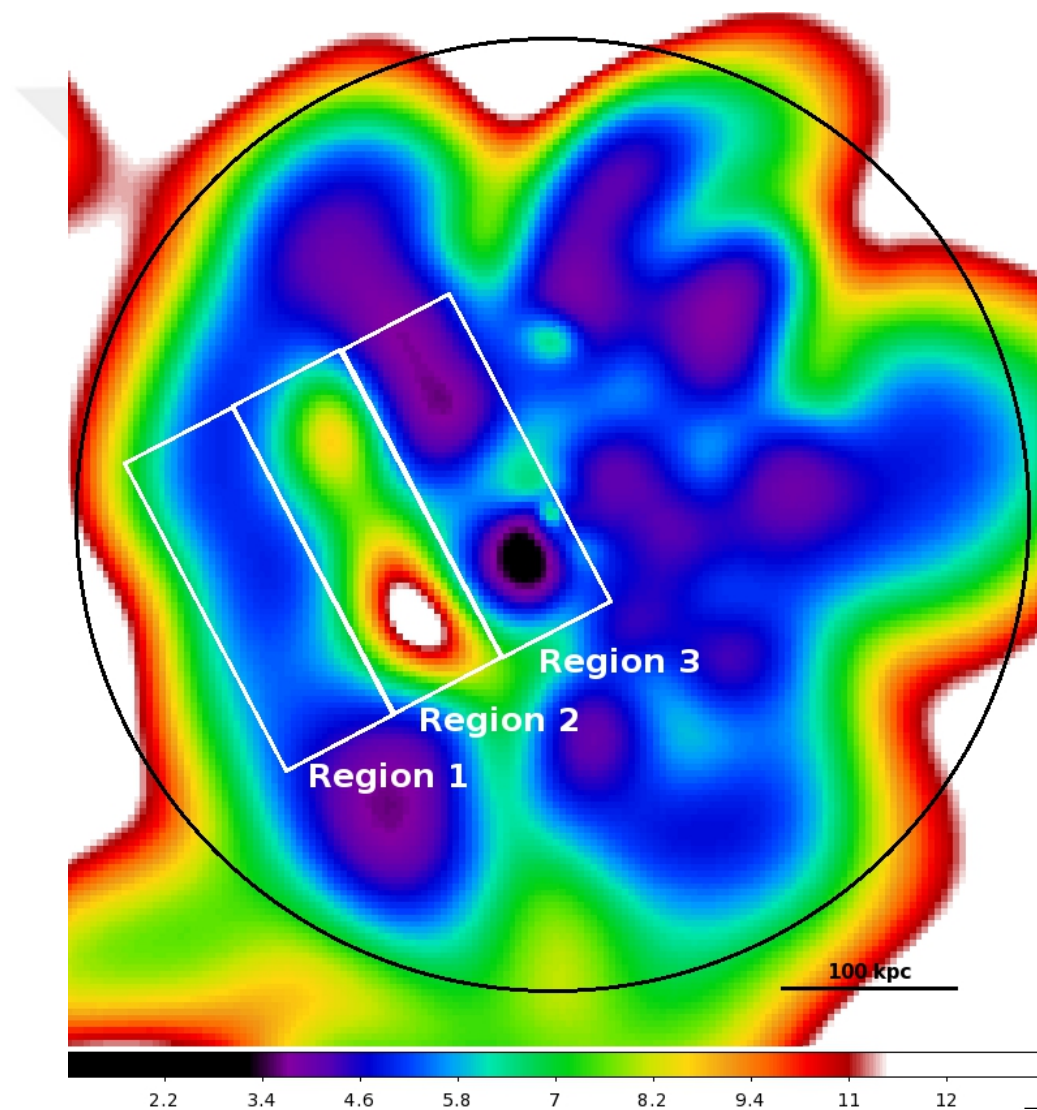


Figure 5.6 Temperature map with possible shock region (region 2), pre-shock region (region 3) and after shock region (region 1)

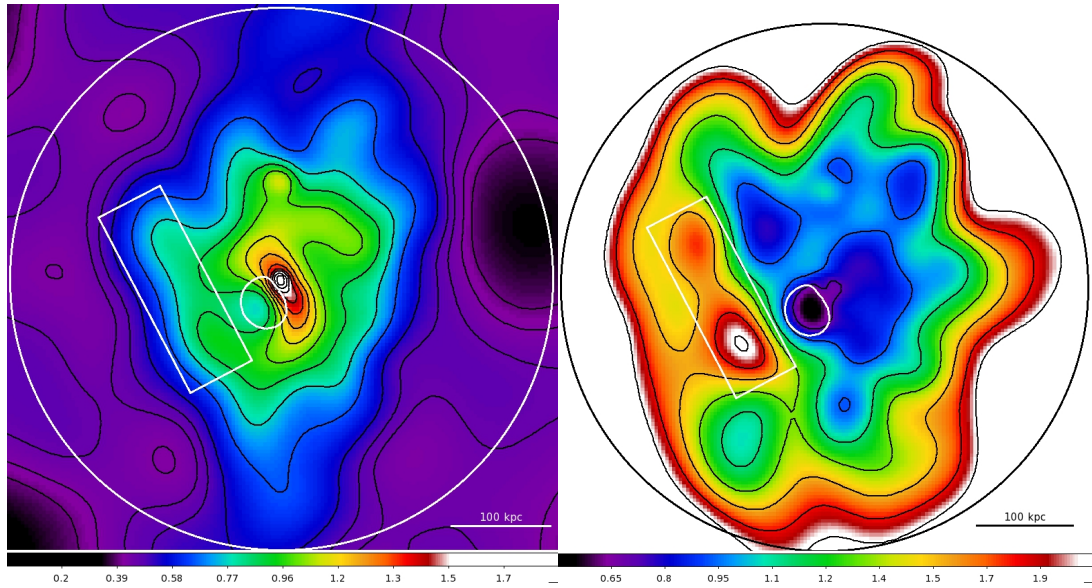


Figure 5.7 Pressure and entropy map with sub-structure regions

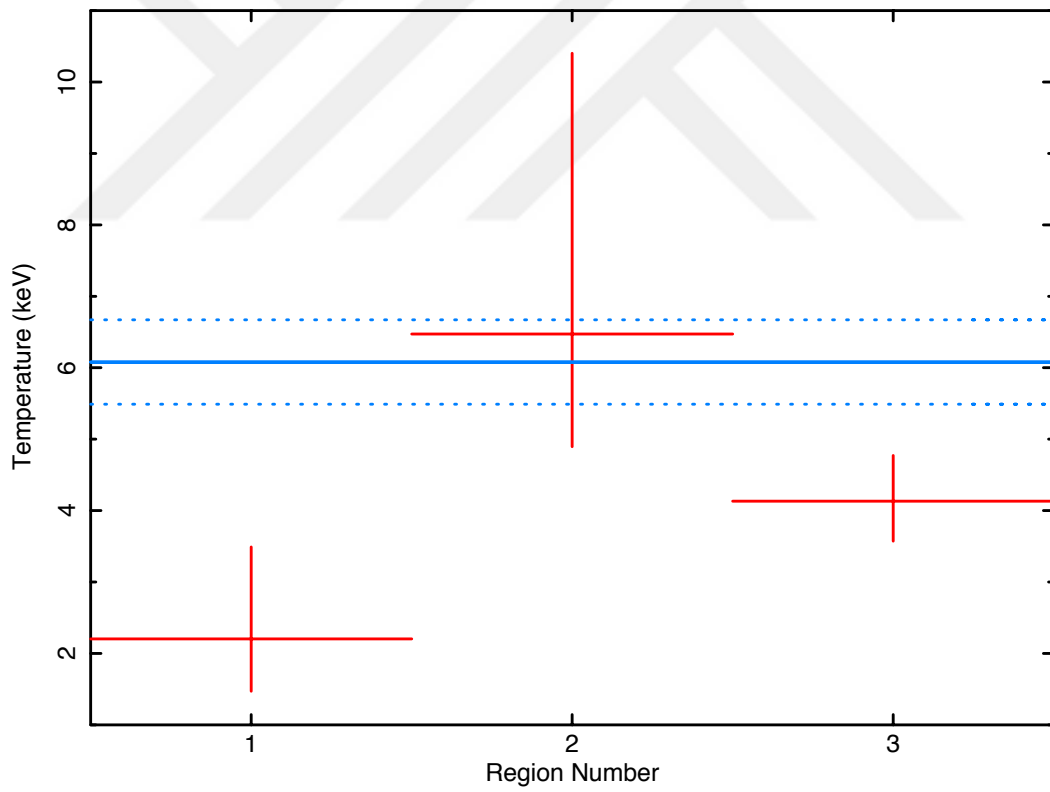


Figure 5.8 Temperature values of Region 1, 2 and 3 showed in Figure 5.6

5.3 Cold Front

In addition to these results, we detected a possible “cold front” between the shock region and the center of the cluster, shown in Figure 5.5 (circular region with white colored). We analyzed this region individually in order to decide if it is a cold front or not. General properties of the cold fronts are discussed in Chapter 1. They are cool and dense gas clouds with low entropy, and traversing through the ICM. We expect to see a surface brightness discontinuity across the cold fronts as in shocks. Cold fronts should have pressure balance with the ambient medium. In this section, we presented the results with the guidance of these properties that expected from a cold front.

The black colored region in Figure 5.9 was selected according to the temperature map as a possible cold-front region. Temperature value is shown in Figure 4.14 (Region Number 1). Pressure map implies that the plasma is in a dynamical state. There is a cavity located at the left side of the region with a nearly constant pressure value, which is unexpected for undisturbed plasma. The region partially coincides to an area that the pressure increases steeply through the cluster center. The rest is located on the cavity. Assuming that the region is a cold-front, as the steepness level is much more through the cluster center than other directions and the rest shows flat distribution, this might give information about movement direction of the cold-front.

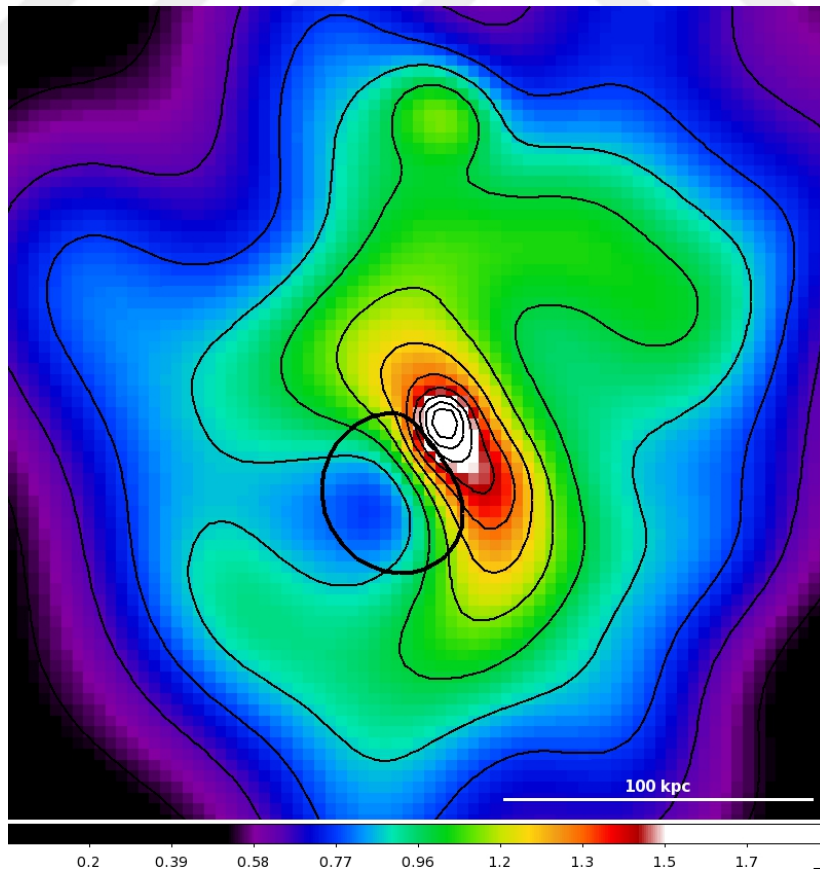


Figure 5.9 Pseudo-pressure map with possible cold-front

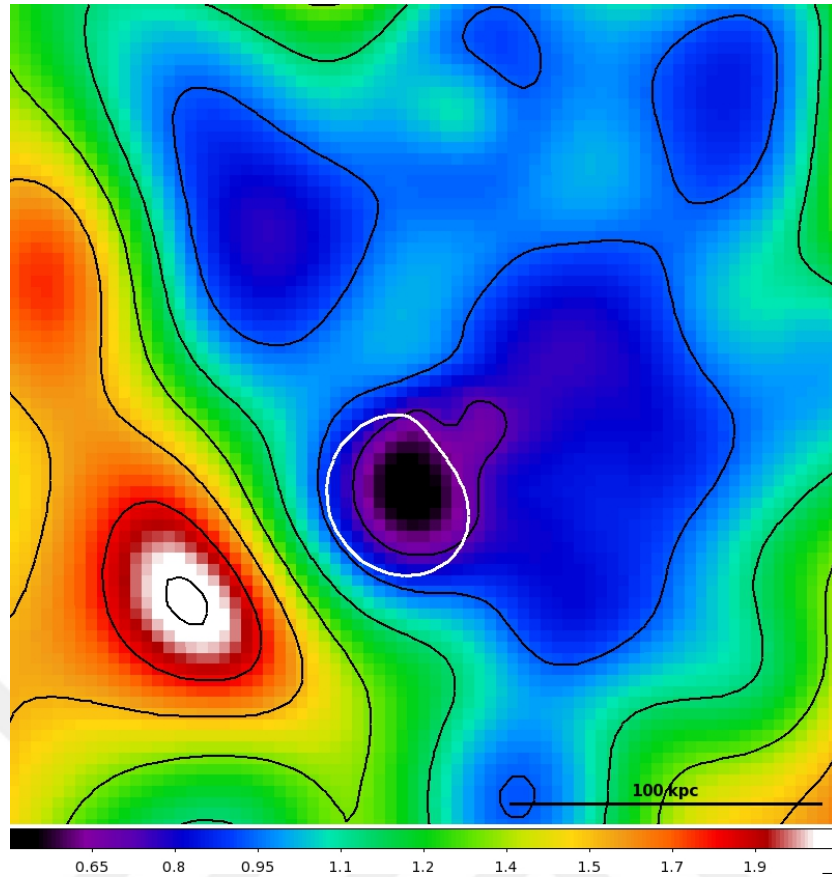


Figure 5.10 Pseudo-entropy map with possible cold-front

Figure 5.10 shows that the possible cold-front is coincide with a low entropy area. This result is what we expect to see for a cold front.

5.4 Conclusion

All of the criterions that we discussed are covered by the shock region. As we know, radio haloes are thought to be produced by mergers [2]. This is the only process known to supply more than sufficient energy over a widespread volume that can easily power the high energy particle population of radio halo [14]. Radio emission that located as in the Figure 4.13 might supports our hypothesis. These results lead us to diagnose the region as a merger shock and A2554 is a part of an ongoing merger process.

Results of the analysis about the possible cold-front region support our hypothesis. Unfortunately, due to low exposure time, we are unable to obtain more confident results. Deeper observations may provide sufficient information about our possible scenarios. Projected view also prevent us to understand the 3D structure of the cluster.

In our study, we only discussed the shock-heated side of the cluster. There are also surface brightness discontinuities along other directions, showed in Figure 4.6 and Figure 4.7. But there aren't any significant temperature changes across those edges. In general, the edges may arise from moving cold gas clouds that are remnants of merger activity. They may arise either from massive mergers, multiple collapses, or oscillations of gas clouds before finally coming to rest. Alternatively, some edges could arise from the interaction of surviving cold, dark matter halos as they move within the cluster potential. As these halos move, they could give rise to the multiple surface brightness edges observed in some clusters [7].



REFERENCES

-
- [1] Paterno-Mahler, R., Randall, S. W., Bulbul, E., Andrade-Santos, F., Blanton, E. L., Jones, C., Murray, S. and Johnson, R. E., (2014). “Merger Signatures in the Galaxy Cluster A98”, *ApJ*, 791:104P
- [2] Feretti, L., Gioia, I. M. and Giovannini, G., (2002), “Merging Processes in Galaxy Clusters”, *ASSL*, 272:F
- [3] Sarazin, C. L., (2002), “The Physics of Cluster Mergers”, *ASSL*, 272, 1S
- [4] Dasadia, S., Sun, M., Morandi, A., Sarazin, C., Clarke, T., Nulsen, P., Massaro, F., Roediger, E., Harris, D. and Forman, B., (2016), “Shocking Features in the Merging Galaxy Cluster RXJ0334.2-0111”, *MNRAS*.tmp, 81D
- [5] Owers, M. S., Nulsen, P. E. J., Couch, W. J., Ma, C., David, L. P., Forman, W. R., Hopkins, A. M., Jones, C. and van Weeren, R. J., (2014), “A Merger Shock in A2034”, *ApJ*, 780:163O
- [6] Henriksen. M. J., Markevitch, M. L., (1996), “Abell 754: A Non-Head-on Collision of Subclusters”, *ApJL*, 466, L79
- [7] Forman, W., Jones, C., Markevitch, M., Vikhlinin, A. and Churazov, E., (2002), “High Angular Resolution Cluster Observations with Chandra”, *ASSL*, 272, 109F
- [8] Russell, H. R., Fabian, A. C., McNamara, B. R., Edge, A. C., Sanders, J. S., Nulsen, P. E. J., Baum, S. A., Donahue, M. and O’Dea, C. P., (2014), “The bow shock, cold fronts and disintegrating cool core in the merging galaxy group RXJ0751.3+5012”, *MNRAS*, 444, 629R
- [9] Markevitch, M., Vikhlinin, A., (2007), “Shocks and Cold Fronts in Galaxy Clusters”, *PhR*, 443, 1M
- [10] Dickey, J. M., & Lockman, F. J., (1990), “H I IN THE GALAXY”, *ARA&A*, 28, 215
- [11] Batuski, D. J., Miller, C. J., Slinglend, K. A., Balkowski, C., Maurogordato, S., Cayatte, V., Felenbok, P. and Olowin, R., (1999), “Discovery of Extreme Examples of Superclustering in Aquarius”, *ApJ*, 520, 491-506
- [12] Smith, R. K., Brickhouse, N. S., Liedahl, D. A. and Raymond, J. C. (2001),

“Collisional plasma models with APEC/APED: Emission-line diagnostics of hydrogen-like and helium-like ions”, *ApJL*, 556, L91

- [13] Briel, U. G., Finoguenov, A. and Henry, J. P., (2004), “XMM-Newton EPIC observation of the galaxy cluster A 3667”, *A&A*, 426:1B
- [14] Landau, L. D., Lifshitz, E. M., (1959), “Fluid Mechanics”, Pergamon Press, London



CURRICULUM VITAE

PERSONAL INFORMATION

Name Surname : Muhammed Kiyami ERDİM
Date of birth and place : 05/10/1988 KADIKOY/ISTANBUL
Foreign Languages : English - Japanese
E-mail : kiyami_erdim@hotmail.com

EDUCATION

Degree	Department	University	Date of Graduation
Master	Physics	Yıldız Technical University	06/2016
Undergraduate	Physics	Marmara University	06/2010